N78-32079

NASA Contractor Report 145356

Strapdown System Redundancy Management Flight Demonstration Final Report

Litton
GUIDANCE & CONTROL SYSTEMS
5500 Canoga Avenue, Woodland Hills, California 91364

CONTRACT No. NAS1-15155
SEPTEMBER 1978

NASA
National Aeronautics and
Space Administration

Langley Research Center
Hampton, Virginia 23665

REPRODUCIBLE COPY
(FACILITY CASEFILE COPY)

TABLE OF CONTENTS

LIST OF ILLUSTRATIONS

LIST OF ILLUSTRATIONS (cont)

LIST OF ILLUSTRATIONS (cont)

LIST OF TABLES

STRAPDOWN SYSTEM REDUNDANCY MANAGEMENT FLIGHT DEMONSTRATION

1.0 INTRODUCTION

The Guidance and Control Systems division of Litton Systems, Inc. conducted a flight test of a tuned-rotor, two-degree-of-freedom gyro strapdown system to evaluate a redundancy management concept. This evaluation was performed under Langley Research Center contract NAS1-15155 in November 1977.

The redundancy management approach evolved from a series of analytical and experimental studies undertaken by Litton as part of an independent research and development program and under contracts to NASA, to McDonnell Douglas Corporation, and to the U.S. Air Force.

A comprehensive treatment of redundancy management using tuned-rotor gyros is given in report NASA CR-145305 entitled "Preliminary Design of a Redundant Strapped Down Inertial Navigation Unit Using Two-Degree-of-Freedom Tuned-Gimbal Gyroscopes" dated October 1976. This report describes the work performed by Litton under contract NAS1-13847 for the Langley Research Center. The purpose of this study was to determine the suitability of strapdown inertial systems in providing highly reliable short-term navigation for vertical take-off and landing (VTOL) aircraft operating in an intra-urban setting under all-weather conditions. A result of this program was a preliminary design configuration of a skewed sensor inertial reference system employing a redundancy management concept to achieve fail-operational, fail-operational performance.

The concept studied under the NASA program was continued under Litton IRAD sponsorship by building and testing a dual inertial measurement unit (IMU) system.

The basic system used was the LN-50 strapdown inertial navigation system (INS) developed and flight tested under IRAD in 1975-1976. The second IMU (skewed) was added in 1976, also under IRAD. Laboratory and road tests of this redundant system (RLN-50) were done as part of the USAF/McDonnell Douglas Multi-Function Inertial Reference Assembly (MIRA) program.

2.0 DESCRIPTION OF TEST PROGRAM

2.1 Objective

The purpose of the NASA/Langley Strapdown Redundancy Management Flight Demonstration was to provide information regarding the software redundancy management capabilities and the demonstration of failure detection and isolation techniques of the Litton RLN-50 System under flight conditions. A description of the RLN-50 System is given in Appendix A.

2.2 Summary of Results

The Litton Redundant Strapdown Inertial Navigator was evaluated in Litton's Merlin IV aircraft from November 11, 1977 through November 18, 1977. Figure 1 shows the test aircraft utilized for this demonstration. A total of five flights were performed along with one ground checkout run. The results obtained from the flight evaluation testing are as follows:

a. The failure detection and isolation techniques of the RLN-50 software were verified in a flight environment by deliberate insertion of faults into the IMU No. 2 (skewed) solution.

b. During the flight demonstration two "false alarms" occurred.

c. The navigation performance of the level solution was approximately 1.0 nm/hr for all flights including the ground checkout run.

The false alarms mentioned above were subsequently determined to be due to the effect of a heading misalignment angle between IMU No. 1 and IMU No. 2. A discussion and analysis of this effect is given in section 4 of this report.

2.3 Conclusions

a. The redundancy management scheme is effective in detecting and isolating failures introduced into the system under flight conditions.

b. A sensitivity of redundant strapdown systems to initial heading misalignment was defined. This effect was determined from an analysis of false alarms observed during the flight test.

Figure 1. Merlin IV Test Aircraft

c. Navigation performance was monitored continuously during flight with position and velocity recorded. The performance was consistent with earlier LN-50 flight tests results, approximately 1.0 nm/hr.

3.0 FLIGHT TEST

3.1 Test Data

Flight test results are summarized in the plotted data of figures 2 thru 7, which show radial position errors from the level IMU solution for each of the 5 flights, and for a static run.

Figure 8 shows the radial position error for the skewed solution for a typical flight (14 November north-south flight). The plots of the gyro and accelerometer parity equations for the same 14 November north-south flight are presented in Appendix B.

3.2 Test Procedures

The RLN-50 system was installed in the Litton Merlin IV aircraft on November 10, 1977. Figure 9 shows the RLN-50 system installation layout in the Merlin IV cargo area and figure 10 shows the installed system. The following day ground checkout was completed and the flight evaluation phase began. The test plan utilized for the ground checkout and flight tests is presented in table I.

Gyro and accelerometer failures were established to provide information using a combination of one gyro and three accelerometers from IMU No. 1 and one gyro from IMU No. 2.

The gyro fault levels were set at 2.4°/h and 0.9°/s while the accelerometer fault levels were set at 1.9 mg and 124 mg. The low level failures (2.4°/h) and 1.9 mg) demonstrated the ability to detect and isolate soft gyro/accelerometer failures which, over a period of time, will degrade navigation performance. The high level failures (0.9°/s and 124 mg), which will affect the performance of a flight control system, were inserted to demonstrate the system's ability to detect and isolate hard gyro/accelerometer failures. Table II summarizes the time to isolate the faults inserted during the test program.

Test flight operations were based at the Van Nuys, California airport. East-West flights were made between VOR stations at Van Nuys and Parker, Arizona. North-South flights were between Van Nuys and Big Sur, California. The box pattern flight was

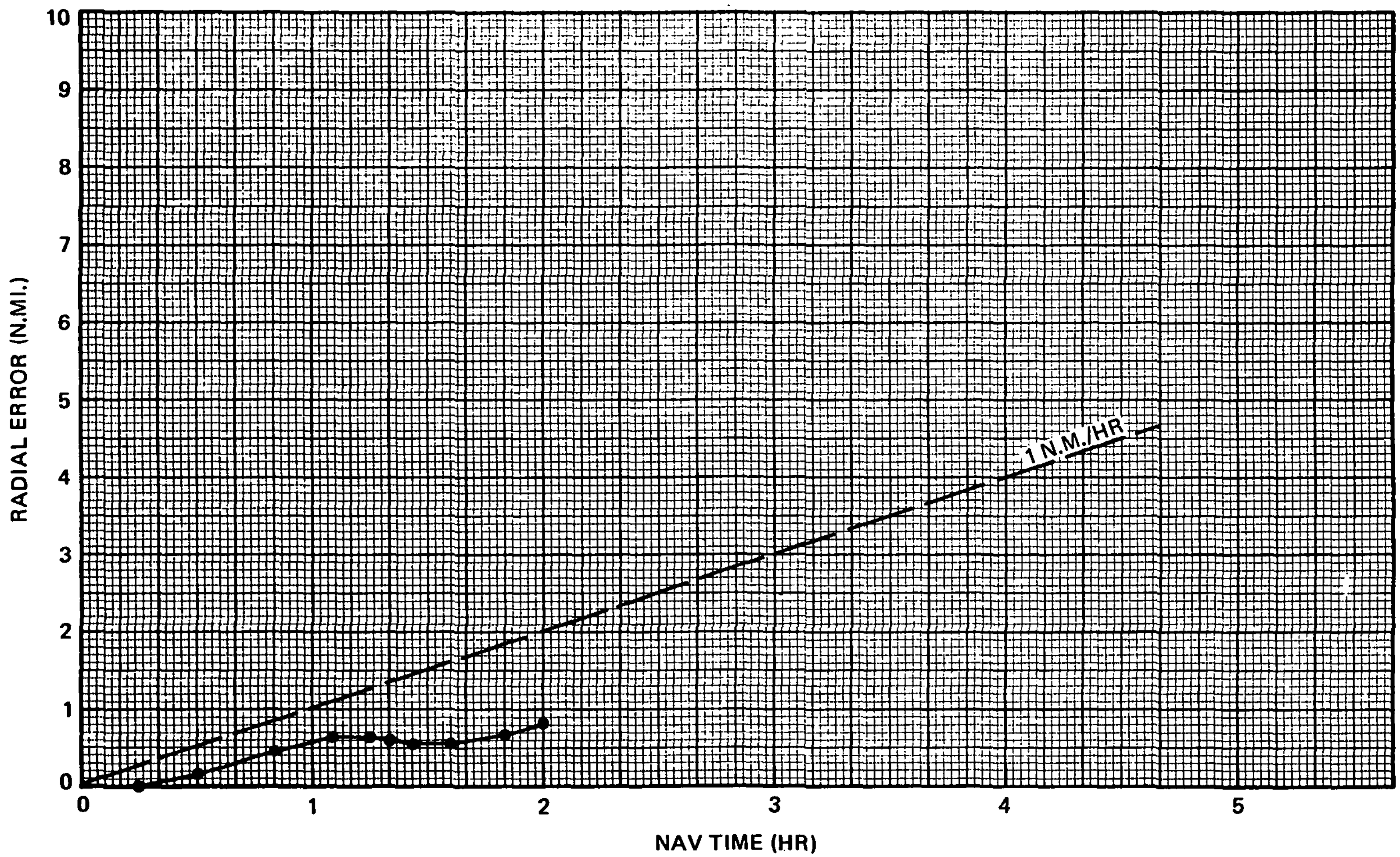

Figure 2. RLN-50 Static Navigation Test (11 November 1977)

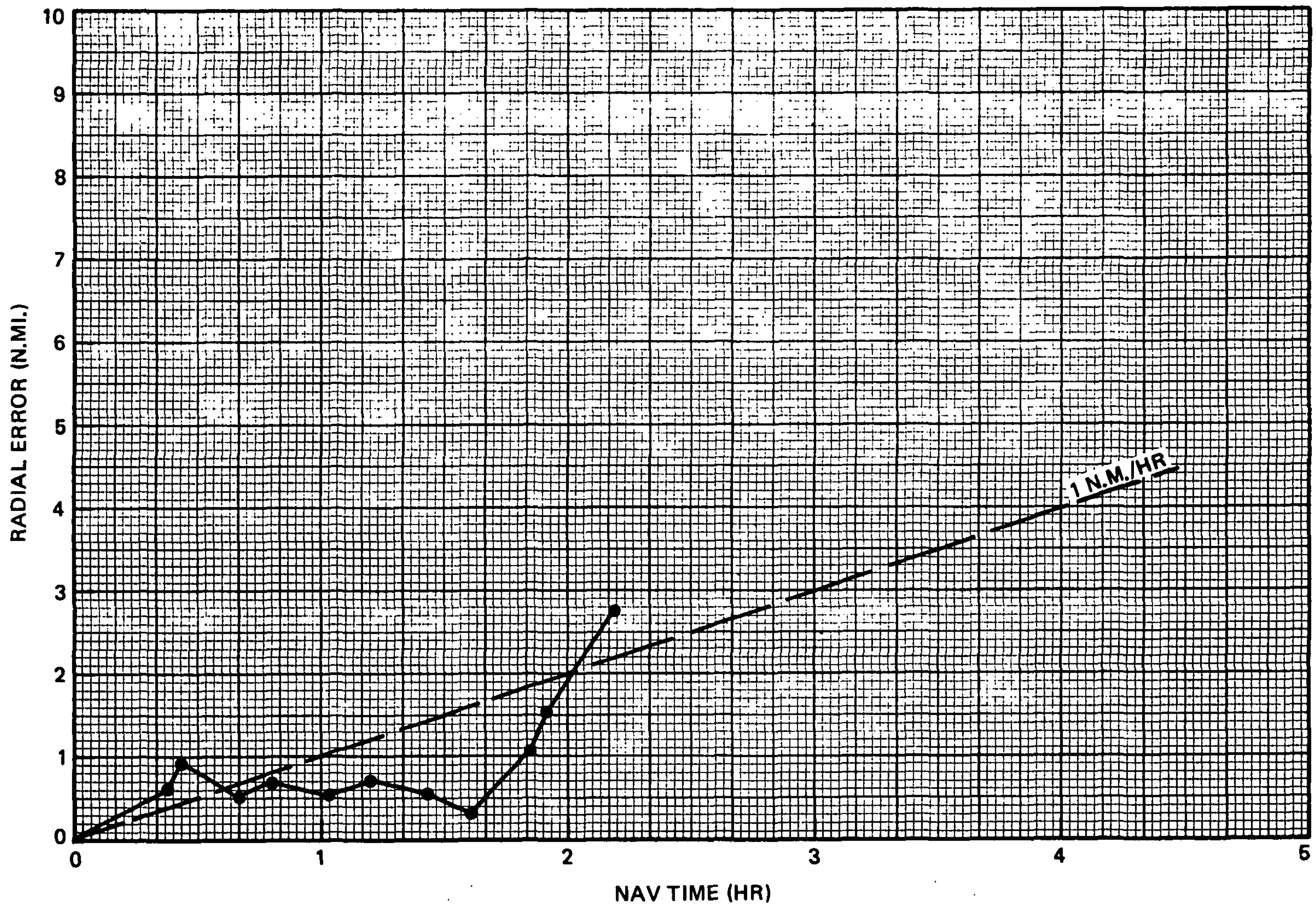

Figure 3. RLN-50 East-West Flight Test (11 November 1977)

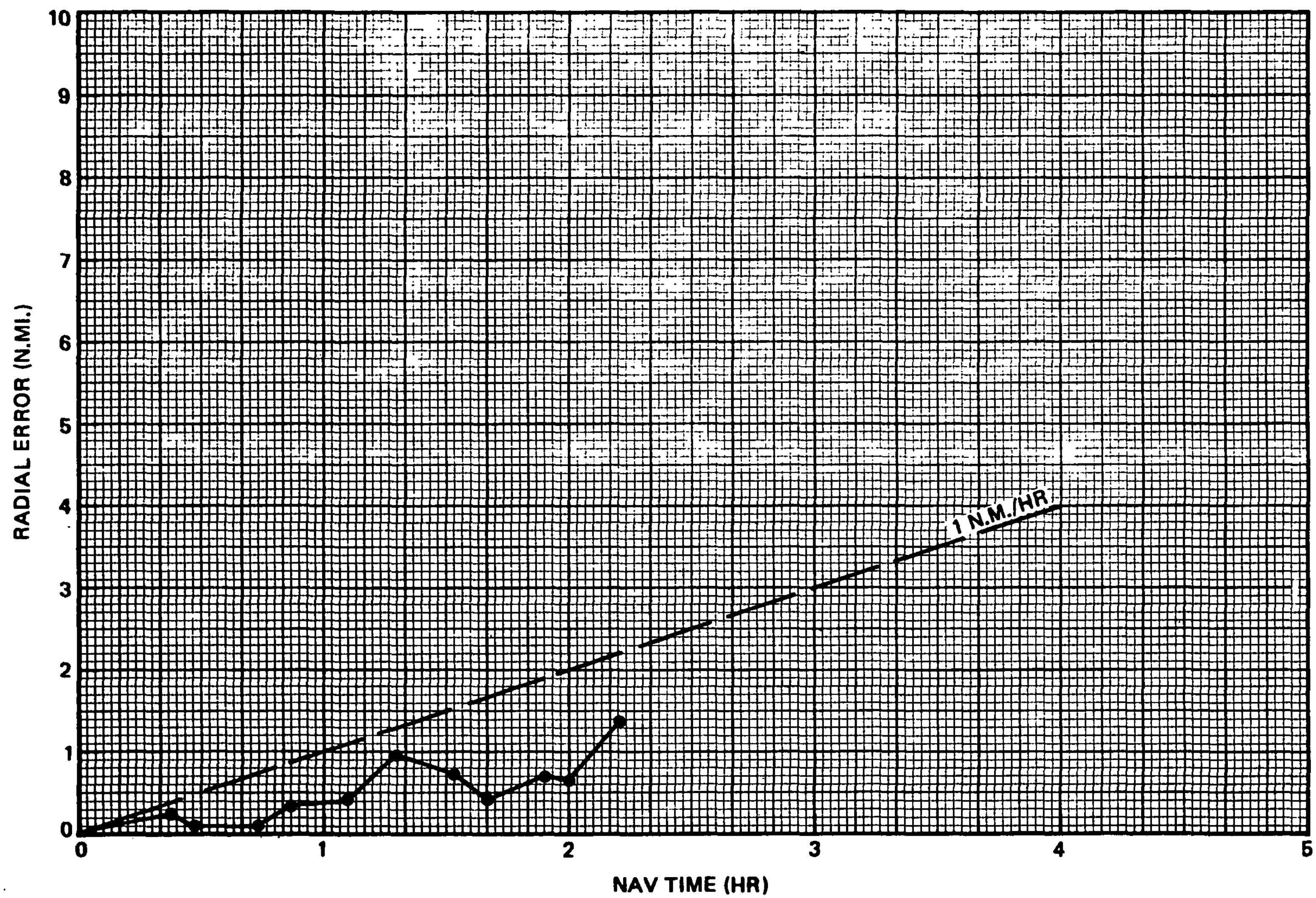

Figure 4. RLN-50 East-West Flight Test (14 November 1977)

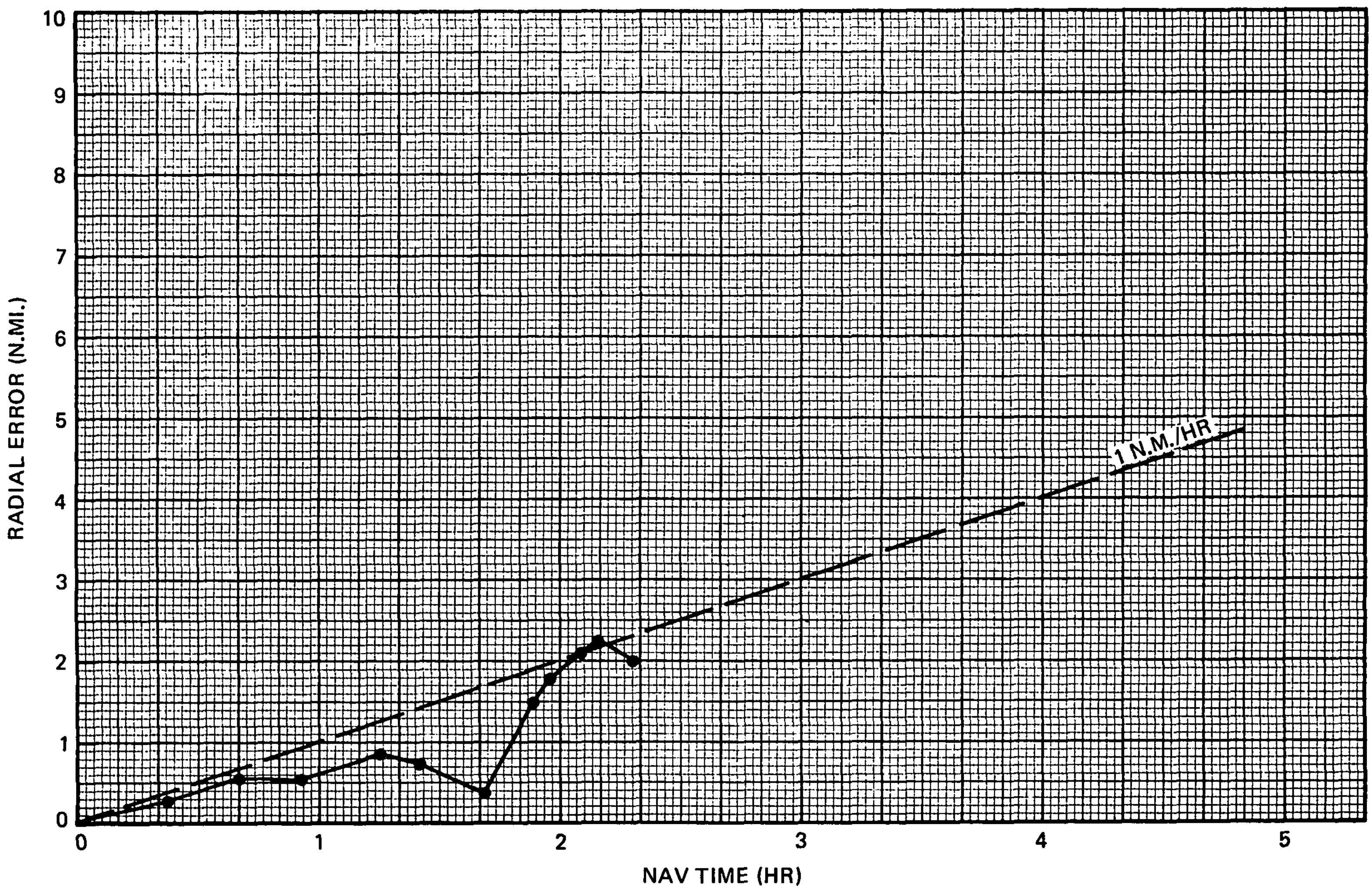

Figure 5. RLN-50 North-South Flight Test (14 November 1977)

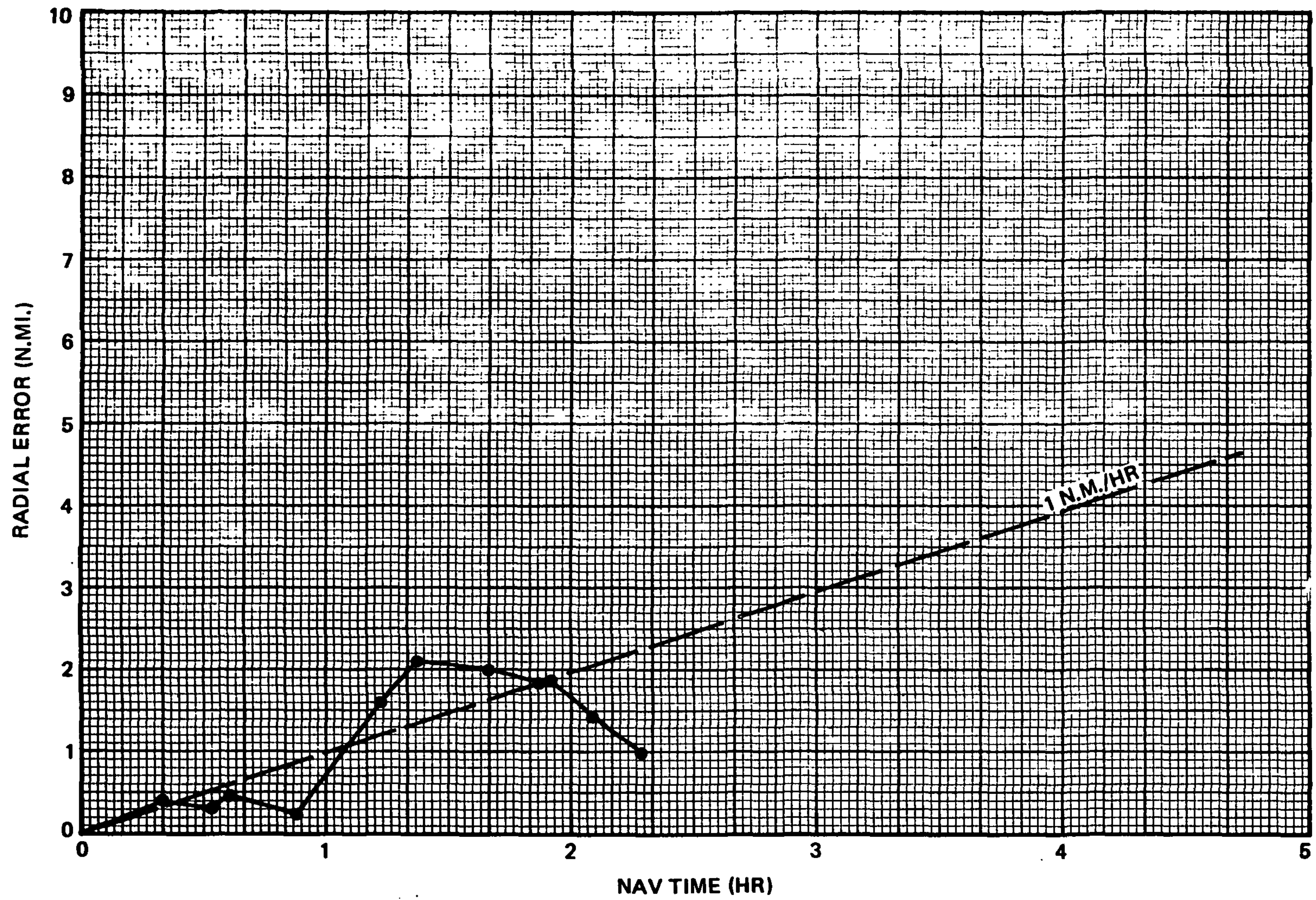

Figure 6. RLN-50 North-South Flight Test (15 November 1977)

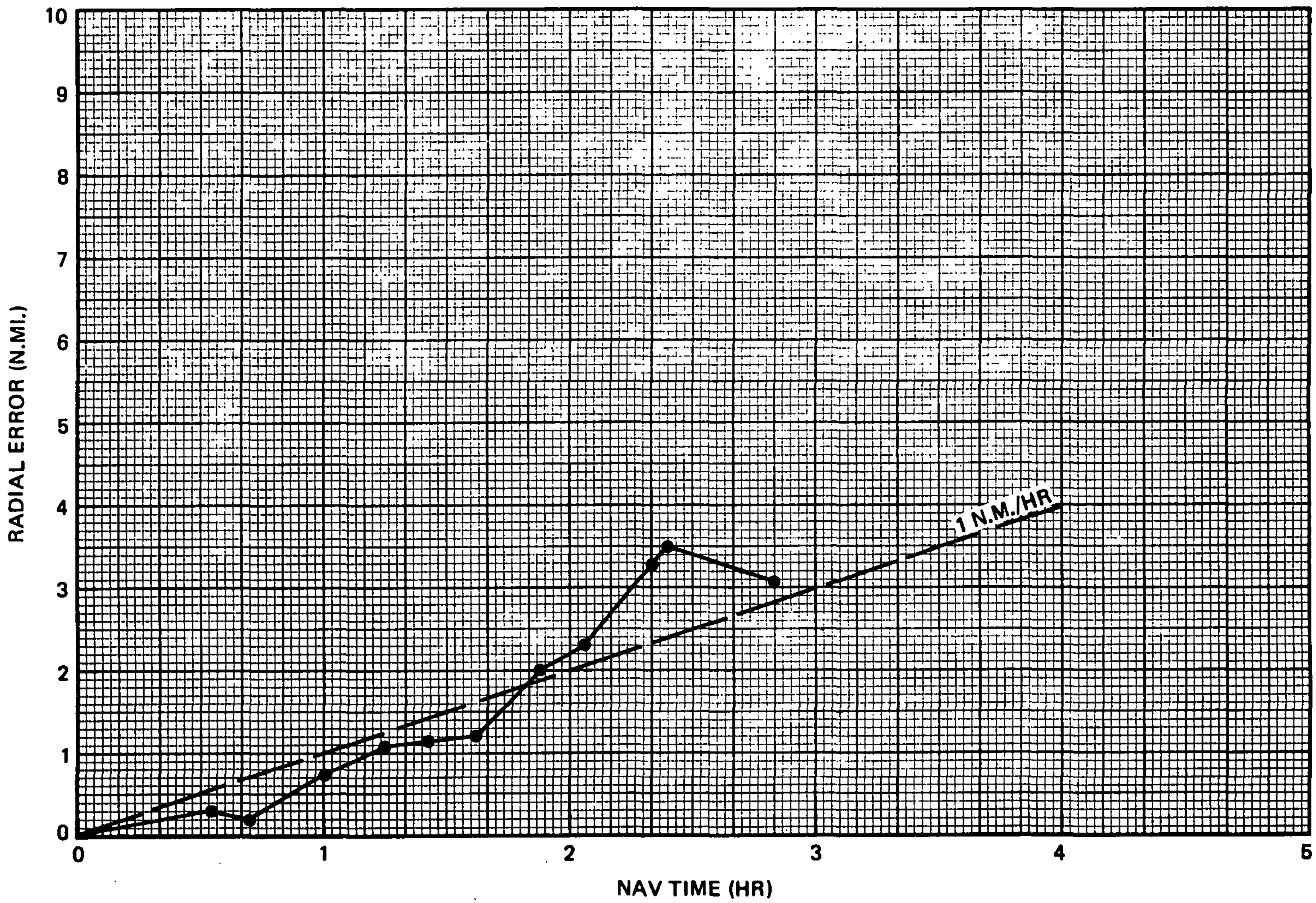

Figure 7. RLN-50 Box Pattern Flight Test (18 November 1977)

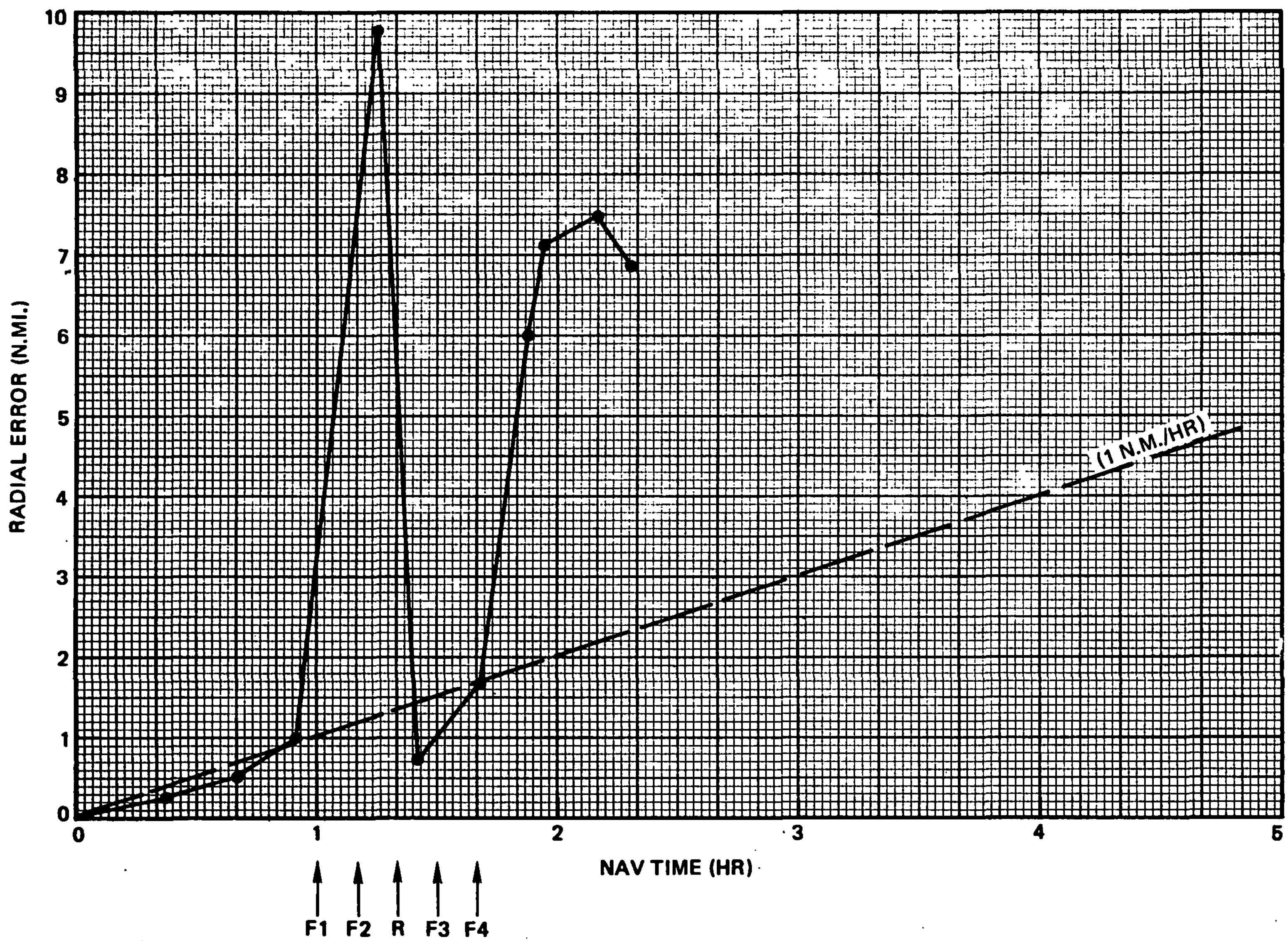

Figure 8. RLN-50 Skewed Solution North-South Flight Test (14 November 1977)

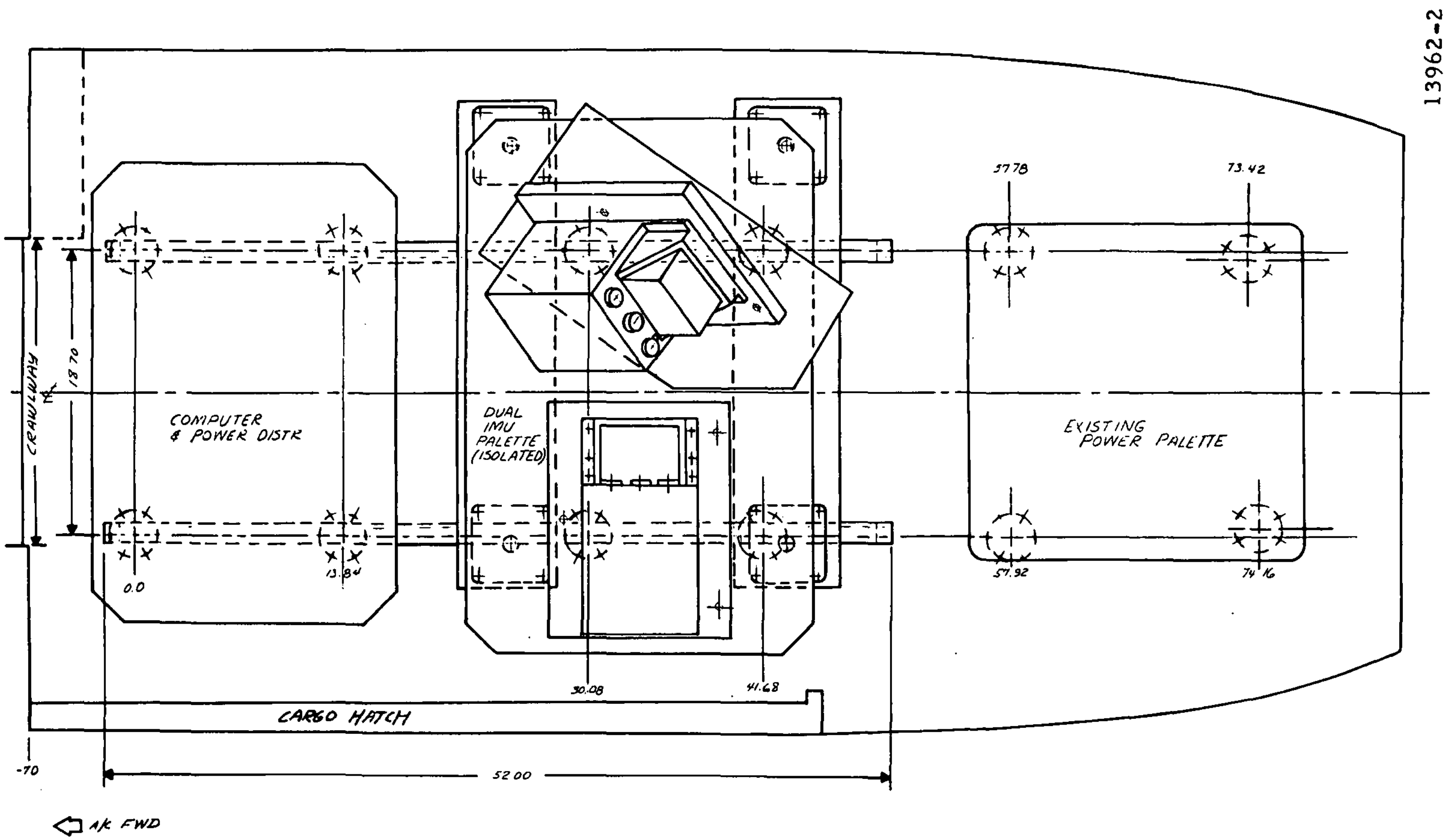

Figure 9. RLN-50 System Installation In Merlin IV Cargo Area

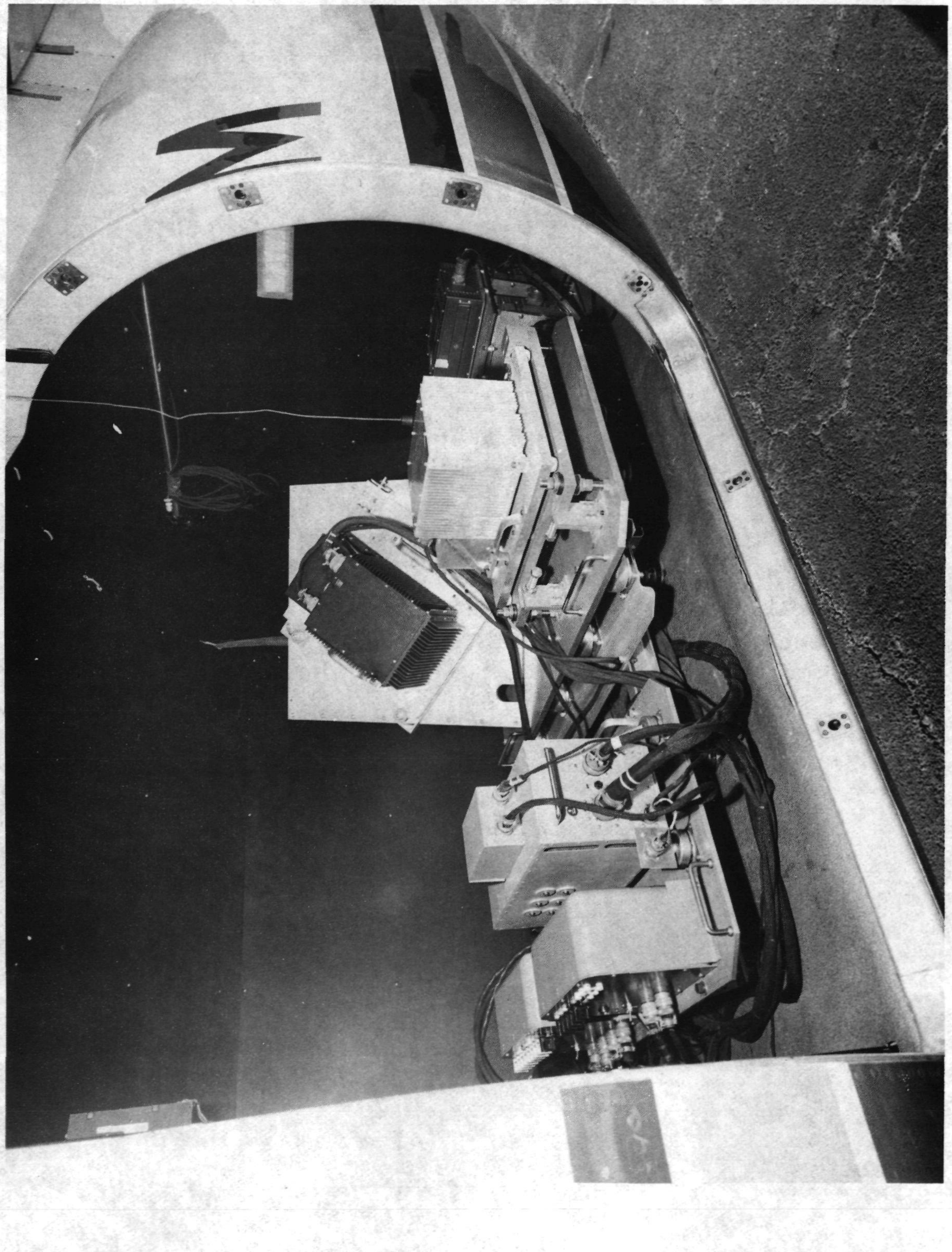

Figure 10. Two LN-50 IMUs on Test Pallet Installed in Test Aircraft

TABLE I. TEST PLAN FOR NASA/LANGLEY FLIGHT DEMONSTRATION

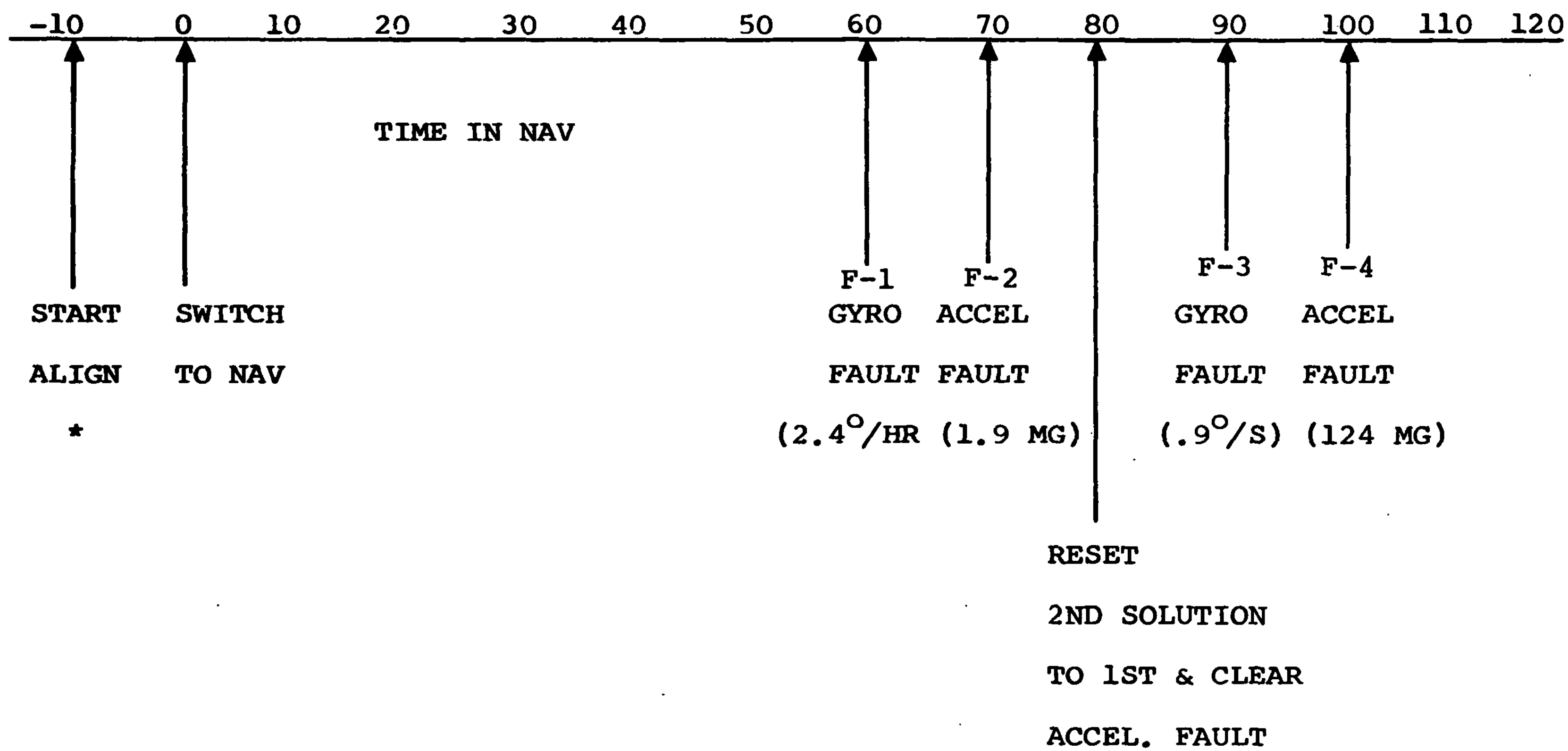

*NOTE: Alternate solution and auto select flags were set at the beginning of the ALIGN mode.

from Van Nuys to Parker to Goffs to Lake Hughes to Van Nuys. All flights were made at a speed of 408 km/hr (220 knots) and at an altitude of 3048 m. (10,000 ft.).

At the conclusion of each flight, the RLN-50 System was allowed to continue running in order to observe the velocity errors that had been generated during the flight. Table III lists the peak X and Y velocity errors generated from the level solution for all flights, including the ground checkout run.

Table IV contains the VOR station checkpoint coordinates for each flight pattern utilized for the RLN-50 demonstration. Table V shows the RLN-50 teletype printout format and table VI shows a sample of the teletype printout.

Testing was completed on November 18, 1977 and the RLN-50 system was removed from the Merlin aircraft.

4.0 ANALYSIS OF PARITY EQUATION FAILURES

During the first flight it was noted that gyro parity equation 1, 4 reached its upper limit, indicating a failure had occurred, while the aircraft was performing a 180 degree turn. The first theory proposed was that bending of the IMU flight pallet, due to g-loading effects during a turn, was causing the attitude adjustment between the IMUs to change, triggering the false alarm.

To minimize possible bending of the pallet, the roll angle of the aircraft was restricted to a maximum of 20 degrees whenever a turn was performed. This approach proved to be successful. One additional false alarm was noted during the final flight, and again, this occurred while the aircraft was executing a turn with a roll angle exceeding 20 degrees. These were the only two false alarms noted during the entire test period.

An investigation into the gyro parity failure which occurred during the test period was initiated following the flight demonstration. The original theory, bending of the flight pallet, was dismissed and another approach was considered. An error in the adjustment of the heading delta between IMU No. 1 and IMU No. 2 was considered as a possible source. The following analysis will show how this error source, coupled with a 180-degree turn and a roll angle of 20 degrees, will cause gyro parity equation 1,4 to fail. Figure 11 represents the input axis for gyro No. 1 (X_1 Y_1) and gyro No. 2 (X_2, Y_2) of the level IMU in the body frame. Assume IMU No. 1 is misaligned from IMU No. 2 in heading by an

TABLE II. ISOLATION TIME AFTER FAULT INSERTION

Flight/Date		Fault Isolation Time (Seconds)			
		F-1	F-2	F-3	F-4
Static	11/11/77	266.02	533.0	0.14	4.5
E-W	11/11/77	279.14	363.0	0.15	4.5
E-W	11/14/77	284.35	381.0	0.15	4.5
N-S	11/14/77	298.22	429.0	0.14	4.5
N-3	11/15/77	390.0	227.0	0.14	4.5
Box	11/18/77	300.0	271.0	0.14	4.5

TABLE III. RLN-50 FLIGHT TEST VELOCITY PEAKS (REFERENCE SOLUTION)

Flight Pattern	X-Velocity	Y-Velocity
East-West	1.83 m/s (6.0 f/s)	-1.34 m/s (-4.4 f/s)
East-West	-0.98 m/s (-3.2 f/s)	-2.71 m/s (-8.9 f/s)
North-South	-0.64 m/s (-2.1 f/s)	-1.13 m/s (-3.7 f/s)
North-South	-2.23 m/s (-7.3 f/s)	1.25 m/s (4.1 f/s)
Box Pattern	-2.74 m/s (-9.0 f/s)	0.95 m/s (3.1 f/s)
Static	-0.03 m/s (-0.1 f/s)	0.49 m/s (1.6 f/s)

TABLE IV. FLIGHT TEST CHECKPOINT COORDINATES

East-West Flight Plan (2.5 Hr. Round Trip)			
VOR Station		Latitude	Longitude
Van Nuys	(VNY)	N 34° -13.4'	W 118° -29.5'
Pomona	(POM)	N 34° -04.7'	W 117° -47.2'
Ontario	(ONT)	N 33° -55.1'	W 117° -31.7'
Palm Springs	(PSP)	N 33° -52.2'	W 116° -25.7'
Twentynine Palms	(TNP)	N 34° -06.7'	W 115° -46.2'
Parker	(PKE)	N 34° -06.1'	W 114° -40.9'
North-South Flight Plan (2.5 Hr. Round Trip)			
VOR Station		Latitude	Longitude
Van Nuys	(VNY)	N 34° -13.4'	W 118° -29.5'
Fillmore	(FIM)	N 34° -21.4'	W 118° -52.8'
Santa Barbara	(SBA)	N 34° -30.6'	W 119° -46.2'
Gaviota	(GVO)	N 34° -31.9'	W 120° -05.6'
Santa Maria	(SMX)	N 34° -57.2'	W 120° -31.2'
San Luis Obispo	(SBP)	N 35° -15.1'	W 120° -45.5'
Big Sur	(BSR)	N 36° -10.0'	W 121° -38.5'

TABLE IV.. FLIGHT TEST CHECKPOINT COORDINATES (cont)

Box Pattern (2.5 Hr. Round Trip)			
VOR Station		Latitude	Longitude
Lake Hughes	(LHS)	N 34° -41.1'	W 118° -34.6'
Palmdale	(PMD)	N 34° -37.9'	W 118° -03.8'
Hector	(HEC)	N 34° -47.8'	W 116° -27.7'
Goffs	(GFS)	N 35° -07.9'	W 115° -10.5'
Needles	(EED)	N 34° -46.0'	W 114° -28.4'
Parker	(PKE)	N 34° -06.1'	W 114° -40.9'
Twentynine Palms	(TNP)	N 34° -06.7'	W 115° -46.2'
Palm Springs	(PSP)	N 33° -52.2'	W 116° -25.7'
Ontario	(ONT)	N 33° -66.1'	W 117° -31.7'
Pomona	(POM)	N 34° -04.7'	W 117° -47.2'
Van Nuys	(VNY)	N 34° -13.4'	W 118° -29.5'

TABLE V. RLN-50 TTY PRINTOUT WITH DEFINITION OF TERMS

TIME (sec)	LAT	LONG	PIT	ROLL	HEAD	ΔLAT	ΔLONG
	←		XXX.XXXX	(DEG)	→	XX.XXXXX (N.M.)	
TIME	R LAT	R LONG	R PIT	R ROLL	R HEAD	R ΔLAT	R ΔLONG
TIME	VN	VE	VY	VX	F TIMER	GXY TEMP	GZR TEMP
	←	XXXX.XXX	(FT/SEC)	→	XXXXX.XX (SEC)	XXX.XXXX	(DEG F)
TIME	R VN	R VE	R VY	R VX	D TIMER	R GXY TEMP	R GZR TEMP
TIME	T_{12}	T_{13}	T_{14}	T_{23}	T_{24}	T_{34}	T_1
	←		X.XXXXXX	(DEG)		→	
TIME	T_2	T_3	T_4	T_5	T_6	T_7	T_8
	←			XX.XXXXX	(FT/SEC)		→
TIME	T_9	B.M.TAG	B.M.TIME	G PARITY	A PARITY	SEL.WORD	SYS STAT
			XXXXX.XX (SEC)	←	XXXXXXX (OCTAL)		→

TIME Instantaneous record of time that system has been navigating or aligning.

LAT Latitude computer by the reference solution

LONG Longitude computed by the reference solution

PIT Pitch angle of reference solution

TABLE V. RLN-50 TTY PRINTOUT WITH DEFINITION OF TERMS (cont)

ROLL	Roll angle of reference solution
HEAD	Heading angle of reference solution
ΔLAT.	Latitude error reference solution
ΔLONG	Longitude error reference solution
R LAT	Latitude computed by the redundant solution
R LONG	Longitude computed by the redundant solution
R PIT	Pitch angle of redundant solution
R ROLL	Roll angle of redundant solution
R HEAD	Heading angle of redundant solution
R ΔLAT	Latitude error redundant solution
R ΔLONG	Longitude error redundant solution
VN	North velocity reference solution
VE	East velocity reference solution
VY	Y-Velocity reference solution
VX	X-Velocity reference solution
F TIMER	Fault insertion time
GXY TEMP	Temperature of X-Y gyro reference IMU
GZR TEMP	Temperature of Z-R gyro reference IMU
R VN	North velocity redundant solution
R VE	East velocity redundant solution
R VY	Y-Velocity redundant solution

TABLE V. RLN-50 TTY PRINTOUT WITH DEFINITION OF TERMS (cont)

R VX	X-Velocity redundant solution
D TIMER	Fault detection time
R GXY TEMP	Temperature of X-Y gyro skewed IMU
R GZR TEMP	Temperature of Z-R gyro skewed IMU
T_{12} - T_{34}	Gyro parity equation responses
T_1 - T_9	Accelerometer parity equation responses
B.M. TAG	Tags each check point that aircraft flew over
B.M. TIME	Represents the time when each check point was flow over
G PARITY	Octal word from computer memory indicating which gyro parity equations have reached the upper limit
A PARITY	Octal word from computer memory indicating which accel. parity equations have reached the upper limit
SEL. WORD	Octal word indicating which design equations are being utilized for the redundant solution
SYS STAT	Octal word indicating system malfunctions if they should occur

TABLE VI. SAMPLE RLN-50 TTY PRINTOUT

0000440	0342083	0000000	0010802	0002590	1791278	-0000142	0004834
0000443	0342083	0000000	0010739	0002548	1792452	-0000301	0008325
0000446	0000082	0000000	-0000001	0000007	0000000	1601274	1607368
0000449	0000062	-0000062	0000016	0000003	0000000	1630571	1620024
0000452	-0001600	-0002633	-0000770	0003470	-0014358	-0010498	-0037336
0000455	-0050590	-0109194	0094995	-0053110	-0125942	0115602	0041632
0000458	-0009397	0000000	0000000	000000	000000	000000	000000
0000461	0342083	0000000	0008821	0002535	1791298	-0000130	0004834
0000464	0342083	0000000	0007703	0002435	1792403	-0000309	0008325
0000467	0000082	0000000	0000002	-0000027	0000000	1597993	1606821
0000470	0000062	0000000	0000006	0000000	0000000	1630961	1619711
0000473	-0001826	-0002662	-0000400	0003107	-0015297	-0010939	-0038812
0000476	-0052131	-0111445	0098050	-0053615	-0128382	0118113	0042458
0000479	-0009675	0000000	0000000	000000	000000	000000	000000
0000482	0342083	0000000	0009449	0002547	1791430	-0000115	0004834
0000485	0342083	0000000	0009352	0002531	1792463	-0000318	0008325
0000488	0000082	0000000	-0000002	-0000002	0000000	1599243	1606899
0000491	0000062	0000000	-0000000	0000000	0000000	1634243	1619086
0000494	-0001923	-0002894	-0000405	0003309	-0015418	-0011417	-0040591
0000497	-0053087	-0113547	0100798	-0054101	-0131695	0121698	0043589
0000500	-0009420	0000000	0000000	000000	000000	000000	000000
0000503	0342083	0000000	0009383	0002623	1791502	-0000111	0009623
0000506	0342083	0000000	0009336	0002579	1792452	-0000324	0003645
0000509	0000082	0000000	-0000002	-0000005	0000000	1603305	1606821
0000512	0000000	0000000	-0000000	-0000002	0000000	1627680	1620571
0000515	-0001998	-0003023	-0001003	0003272	-0015910	-0011727	-0042751
0000518	-0054133	-0114780	0102987	-0054005	-0134095	0124760	0044298
0000521	-0008548	0000000	0000000	000000	000000	000000	000000
0000524	0342083	0000000	0009386	0002615	1791595	-0000109	0009623
0000527	0342083	0000000	0009393	0002566	1792461	-0000328	0003645
0000530	0000019	-0000062	-0000003	-0000002	0000000	1602446	1606431
0000533	0000062	-0000062	-0000002	-0000004	0000000	1621977	1621196
0000536	-0001717	-0002777	-0000518	0003320	-0015876	-0011846	-0044411
0000539	-0055391	-0116435	0105744	-0054455	-0136343	0127531	0045158
0000542	-0007773	0000000	0000000	000000	000000	000000	000000
0000545	0342083	0000000	0009449	0002608	1791634	-0000105	0009623
0000548	0342083	0000000	0009386	0002582	1792457	-0000332	0003645
0000551	0000019	0000000	-0000001	0000004	0000000	1604555	1607446
0000554	0000000	-0000062	0000001	-0000000	0000000	1627289	1621040
0000557	-0001935	-0002721	-0000582	0003285	-0016202	-0012099	-0046319
0000560	-0056555	-0117703	0108133	-0054417	-0137929	0129577	0045400
0000563	-0006895	0000000	0000000	000000	000000	000000	000000
0000566	0342083	0000000	0009446	0002613	1791678	-0000107	0009623
0000569	0342083	0000000	0009400	0002568	1792488	-0000338	0003645
0000572	0000019	0000000	0000001	-0000000	0000000	1599633	1607290
0000575	0000124	0000000	0000000	0000005	0000000	1633383	1620961
0000578	-0002399	-0002763	-0000540	0003392	-0016833	-0011996	-0047972
0000581	-0057483	-0118802	0110488	-0053599	-0140359	0132471	0046236
0000584	-0006160	0000000	0000000	000000	000000	000000	000000
0000587	0342083	0000000	0009454	0002607	1791702	-0000107	0009623
0000590	0342083	0000000	0009388	0002572	1792510	-0000339	0003645
0000593	0000019	0000000	-0000004	0000000	0000000	1601274	1607524
0000596	0000062	0000000	-0000003	0000014	0000000	1620414	1620258
0000599	-0002075	-0002573	-0000629	0003530	-0017025	-0012429	-0049888
0000602	-0058458	-0120341	0112184	-0053578	-0142911	0135828	0046954

angle, β. Equation set (1) represents what each gyro will sense assuming β is equal to zero, while equation set (2) is an approximation of what each gyro will sense assuming an angle β. By substituting equation set (2) into the gyro parity equations (see Appendix A) equation set (3) is obtained. If we now assume a roll angle -R and a heading change H and substitute these variables into equations T_{13}-T_{24} from set (3) the final result is obtained in equation set (4). Note that the greatest effect will be to gyro parity equation T_{14}. Using parity equation T_{14}, the value of β needed to cause a parity failure was found to be approximately 1.6×10^{-3} radians (0.092 deg.).

An experiment was performed in the laboratory using the RLN-50 system to verify the above analysis. IMU No. 1 was misaligned from IMU No. 2 in heading by a known angle (β). Gyro parity equations T_{13}, T_{14} were monitored while the IMU flight pallet was rotated in roll and then heading. The results of this experiment are tabulated in table VII.

The observed parity equation failures (false alarms) are thus explained as due to initial heading misalignment.

Only the heading misalignment angle between IMU No. 1 and IMU No. 2 was of sufficient magnitude to affect gyro parity equations. This misalignment had no significant effect on accelerometer parity equations as shown in Figures B-7 thru B-15 of Appendix B.

Flight path had no effect on parity equations, but turns did affect parity equations due to the previously discussed heading misalignment error.

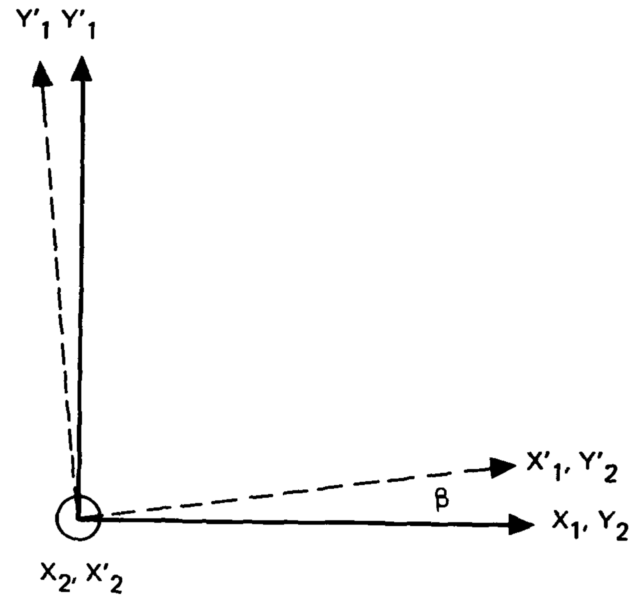

(1) $X_1 = (1, 0, 0)\ X, Y, Z$

$Y_1 = (0, 1, 0)\ X, Y, Z$

$X_2 = (0, 0, 1)\ X, Y, Z$

$Y_2 = (1, 0, 0)\ X, Y, Z$

(2) $X_1' = (1, B, 0)\ X, Y, Z$

$Y_1' = (-B, 1, 0)\ X, Y, Z$

$X_2' = (0, 0, 1)\ X, Y, Z$

$Y_2' = (1, B, 0)\ X, Y, Z$

(3) T_{12} = NO EFFECT

$T_{13} = -B/\sqrt{3}(\sqrt{2}, 1, 0)$

$T_{14} = -B/\sqrt{3}(-\sqrt{2}, 1, 0)$

$T_{23} = B/\sqrt{3}(0, 1, 0)$

$T_{24} = B/\sqrt{3}(0, 1, 0)$

T_{34} = NO EFFECT

(4) $T_{13} = -B/\sqrt{3}(\sqrt{2})\ H\sin R + B/\sqrt{3}(R)$

$T_{14} = +B/\sqrt{3}(\sqrt{2})\ H\sin R + B/\sqrt{3}(R)$

$T_{23} = -B/\sqrt{3}(R)$

$T_{24} = -B/\sqrt{3}(R)$

Figure 11. Input Axes for Level IMU Gyros No. 1 and No. 2

TABLE VII. SUMMARY OF RLN-50 LABORATORY TESTING

Roll Angle R $\cong 10^{\circ}$		
Gyro Parity Equation	Predicted Results	Test Results
T_{13}	$+.030^{\circ}$	$+.034^{\circ}$
T_{14}	$+.030^{\circ}$	$+.034^{\circ}$
Roll Angle R $\cong 10^{\circ}$ Heading Change H $\cong 90^{\circ}$		
Gyro Parity Equation	Predicted Results	Test Results
T_{13}	$-.036^{\circ}$	$-.049^{\circ}$
T_{14}	$+.096^{\circ}$	$+.096^{\circ}$

NOTE: Misalignment Angle $\beta \cong 0.3^{\circ}$

APPENDIX A

LITTON RLN-50 DEMONSTRATION

SYSTEM DESCRIPTION

LITTON RLN-50 DEMONSTRATION
SYSTEM DESCRIPTION

The Litton Strapdown Redundant Inertial Navigator utilizes two orthogonal inertial measurement units (IMU) and one computer, with suitable readout provisions. The hardware is Litton's LN-50 Demonstration Strapdown Inertial Navigation System, mechanized using two G-6 turned rotor gyros and three A-1000 accelerometers in each IMU.

A second IMU is added to the LN-50 to achieve the redundant system. This second IMU is skewed relative to the first so that full three-dimensional information is available with failures of one or two gyros or accelerometers.

Figure A-1 shows the installation of the two IMUs on the pallet. The skew angle is produced by a 90° rotation, as shown in figure A-2, such that the four gyro spin axis, Y, Z, Y', and Z' are equally spaced about a 90° cone.

The outputs of the two IMUs are input to the same LN-50 computer. The software in that computer is structured as shown in figure A-3. The predictable errors of each instrument are removed by compensation at an iteration rate of 64 Hz. Provision for simulating gyro or accelerometer errors is included. These simulated faults are manually injected by means of the LN-50 control display unit. The resulting redundant measurements are compared in failure detection and isolation equations to determine which measurement is in error. The form of these FDI equations, filtering, and logic, solved at a 64 Hz rate, are shown in figures A-4 and A-5 for gyro and accelerometer measurements, respectively.

Two completely separate strapdown solutions are then formed. One is a reference solution using the nonskewed IMU without instrument faults injected. The second solution is based on selectable (manual or automatic via FDI results) pairs of gyros and sets of accelerometers. Design equations perform coordinate transformations and account for the redundant measurement data contained in two two-degree-of-freedom gyros. Two separate sets of quaternion coordinate transformations and inertial navigation equations are then available for comparison. Transients induced into the second solution by manual fault insertion prior to FDI response are then directly observable.

Figures A-6 and A-7 define instrument geometry and coordinate systems.

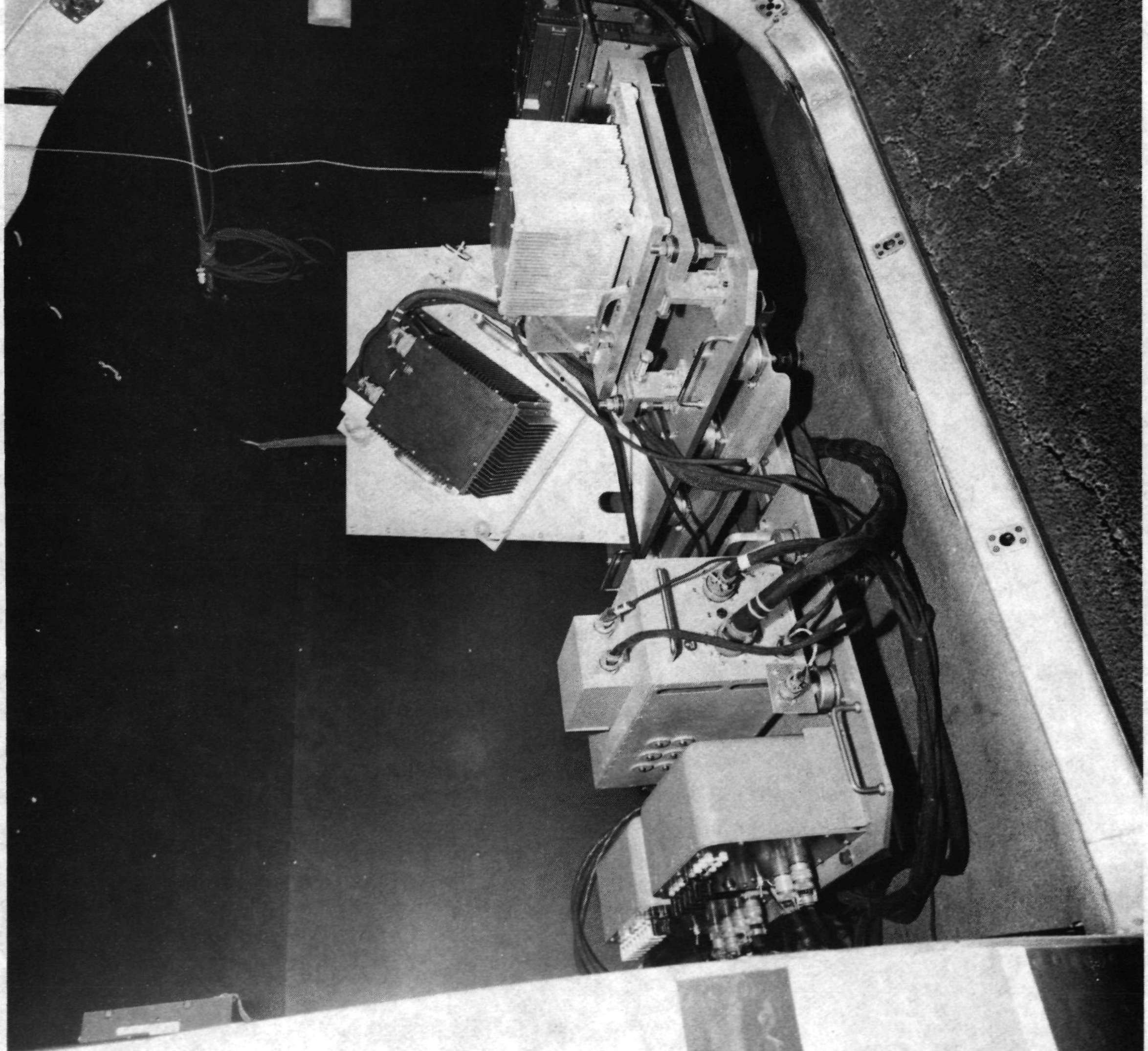

Figure A-1. Two Strapdown IMU's Attached to a Pallet With One IMU Skewed

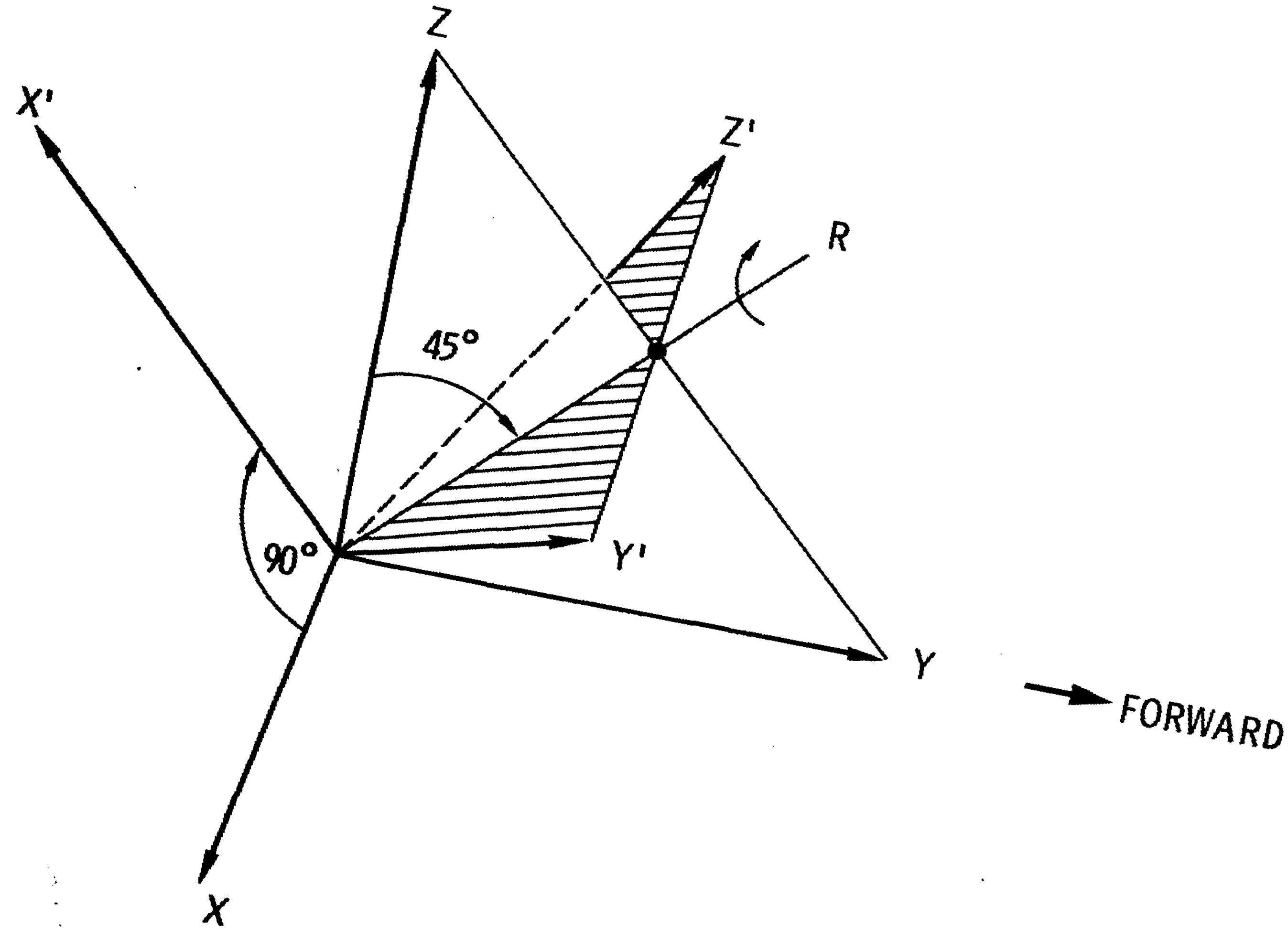

Figure A-2. Dual IMU Geometry

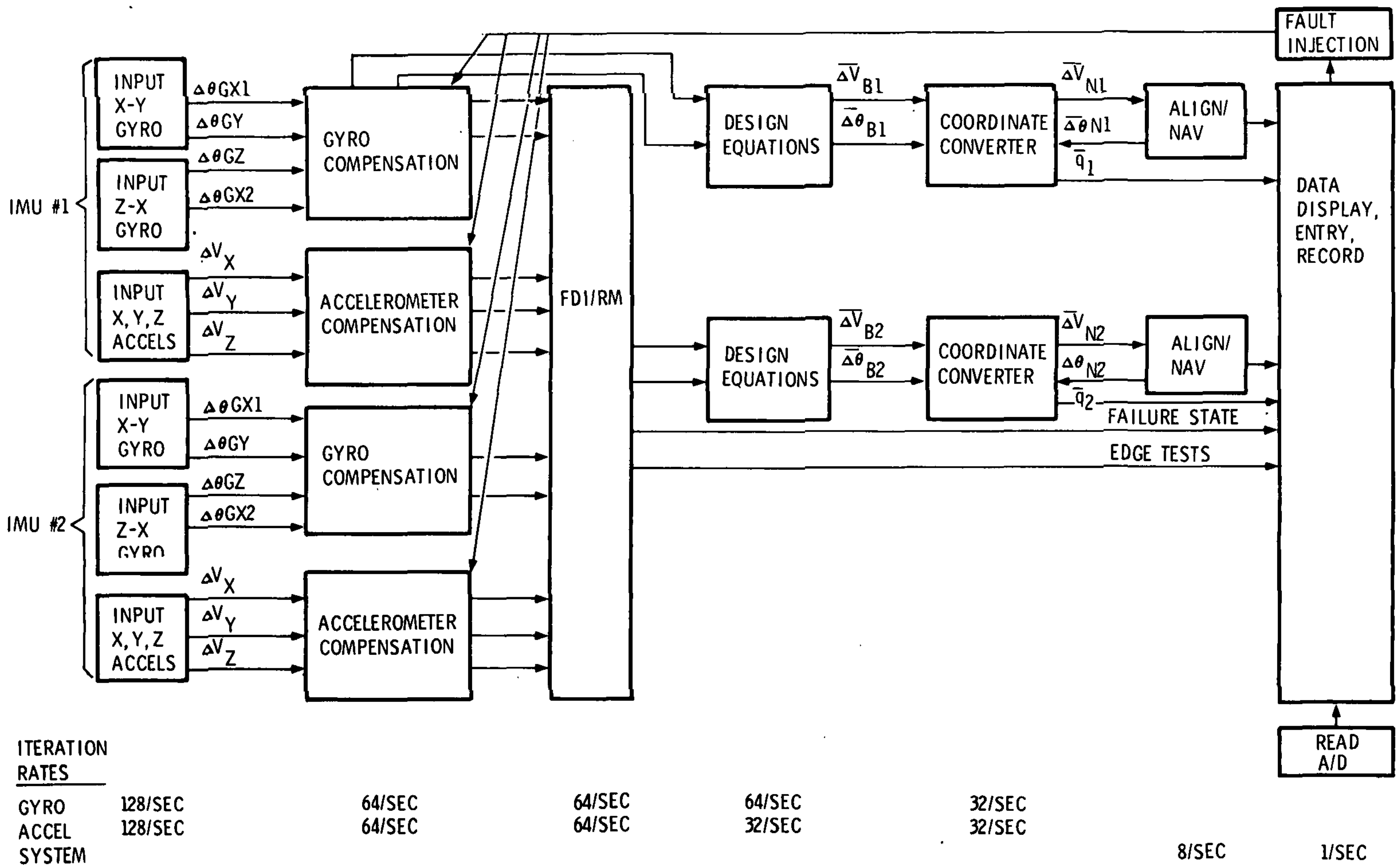

Figure A-3. Dual IMU Demonstration Software Mechanization

GYRO PARITY EQUATIONS - 64/SEC

$$T_{ij} = (\Delta\vec{\theta}^{i} - \Delta\vec{\theta}^{j}) \cdot \vec{e}_{ij}$$

$$T_{12} = - \quad (\Delta\theta_X^{1} - \Delta\theta_Y^{2})$$

$$T_{13} = \frac{1}{\sqrt{3}}\left[- (\Delta\theta_X^{1} - \Delta\theta_Y^{3}) + \sqrt{2} (\Delta\theta_Y^{1} - \Delta\theta_X^{3})\right]$$

$$T_{14} = \frac{1}{\sqrt{3}}\left[- (\Delta\theta_X^{1} + \Delta\theta_X^{4}) - \sqrt{2} (\Delta\theta_Y^{1} - \Delta\theta_Y^{4})\right]$$

$$T_{23} = \frac{1}{\sqrt{3}} \quad \left[\Delta\theta_Y^{2} + \Delta\theta_Y^{3} - \sqrt{2} (\Delta\theta_X^{2} - \Delta\theta_X^{3})\right]$$

$$T_{24} = \frac{1}{\sqrt{3}} \quad \left[\Delta\theta_Y^{2} - \Delta\theta_X^{4} + \sqrt{2} (\Delta\theta_X^{2} - \Delta\theta_Y^{4})\right]$$

$$T_{34} = \Delta\theta_Y^{3} - \Delta\theta_X^{4}$$

NOTE: SUPERSCRIPT DESIGNATES GYRO NUMBER

FILTERING - 64/SEC

$$I_{12} = i_{12} + T_{12} - K_1^{\circ} I_{12}$$

$$I_{13} = I_{13} + T_{13} - K_2^{\circ} I_{13}$$

$$I_{14} = I_{14} + T_{14} - K_3^{\circ} I_{14}$$

$$I_{23} = I_{23} + T_{23} - K_4^{\circ} I_{23}$$

$$I_{24} = I_{24} + T_{24} - K_5^{\circ} I_{24}$$

$$I_{34} = I_{34} + T_{34} - K_6^{\circ} I_{34}$$

THRESHOLD DETECT - 64/SEC

$$\text{IF } (|I_{12}| > \epsilon_1)\ L_{12} = 1$$

$$\text{IF } (|I_{13}| > \epsilon_2)\ L_{13} = 1$$

$$\text{IF } (|I_{14}| > \epsilon_3)\ L_{14} = 1$$

$$\text{IF } (|I_{23}| > \epsilon_4)\ L_{23} = 1$$

$$\text{IF } (|I_{24}| > \epsilon_5)\ L_{24} = 1$$

$$\text{IF } (|I_{34}| > \epsilon_6)\ L_{34} = 1$$

FAILURE ISOLATION - 64/SEC

$$L_1 = (L_{12} \cdot L_{13}) \cdot (\overline{L_2} \cdot \overline{L_3}) + L_{12} \cdot L_{14}) \cdot (\overline{L_2} \cdot \overline{L_4}) + L_{13} \cdot L_{14}) \cdot (\overline{L_3} \cdot \overline{L_4})$$

$$L_2 = (L_{12} \cdot L_{23}) \cdot (\overline{L_1} \cdot \overline{L_3}) + (L_{12} \cdot L_{24}) \cdot (\overline{L_1} \cdot \overline{L_4}) + (L_{23} \cdot L_{24}) \cdot (\overline{L_3} \cdot \overline{L_4})$$

$$L_3 = L_{23} \cdot L_{34}) \cdot (\overline{L_2} \cdot \overline{L_4}) + (L_{13} \cdot L_{34}) \cdot (\overline{L_1} \cdot \overline{L_4}) + (L_{23} \cdot L_{13}) \cdot (\overline{L_1} \cdot \overline{L_2})$$

$$L_4 = (L_{14} \cdot L_{24}) \cdot (\overline{L_1} \cdot \overline{L_2}) + (L_{14} \cdot L_{34}) \cdot (\overline{L_1} \cdot \overline{L_3}) + (L_{24} \cdot L_{34}) \cdot (\overline{L_2} \cdot \overline{L_3})$$

$$L_A = L_{12} \cdot (\overline{L_1} \cdot \overline{L_2}) + L_{13} \cdot (\overline{L_1} \cdot \overline{L_3}) + L_{14} \cdot (\overline{L_1} \cdot \overline{L_4}) + L_{23} \cdot (\overline{L_2} \cdot \overline{L_3})$$
$$+ L_{24} \cdot (\overline{L_2} \cdot \overline{L_4}) + L_{34} \cdot (\overline{L_3} \cdot \overline{L_4})$$

NOTE: · = LOGICAL AND, + = LOGICAL OR

GYRO SELECT - 64/SEC

DES EQN	L_1	L_2	L_3	L_4
34	0	0	0	0
34	1	0	0	0
34	0	1	0	0
14	0	0	1	0
13	0	0	0	1
34	1	1	0	0
24	1	0	1	0
23	1	0	0	1
14	0	1	1	0
13	0	1	0	1

Figure A-4. Gyro Failure Detection, Isolation and Selection Equations

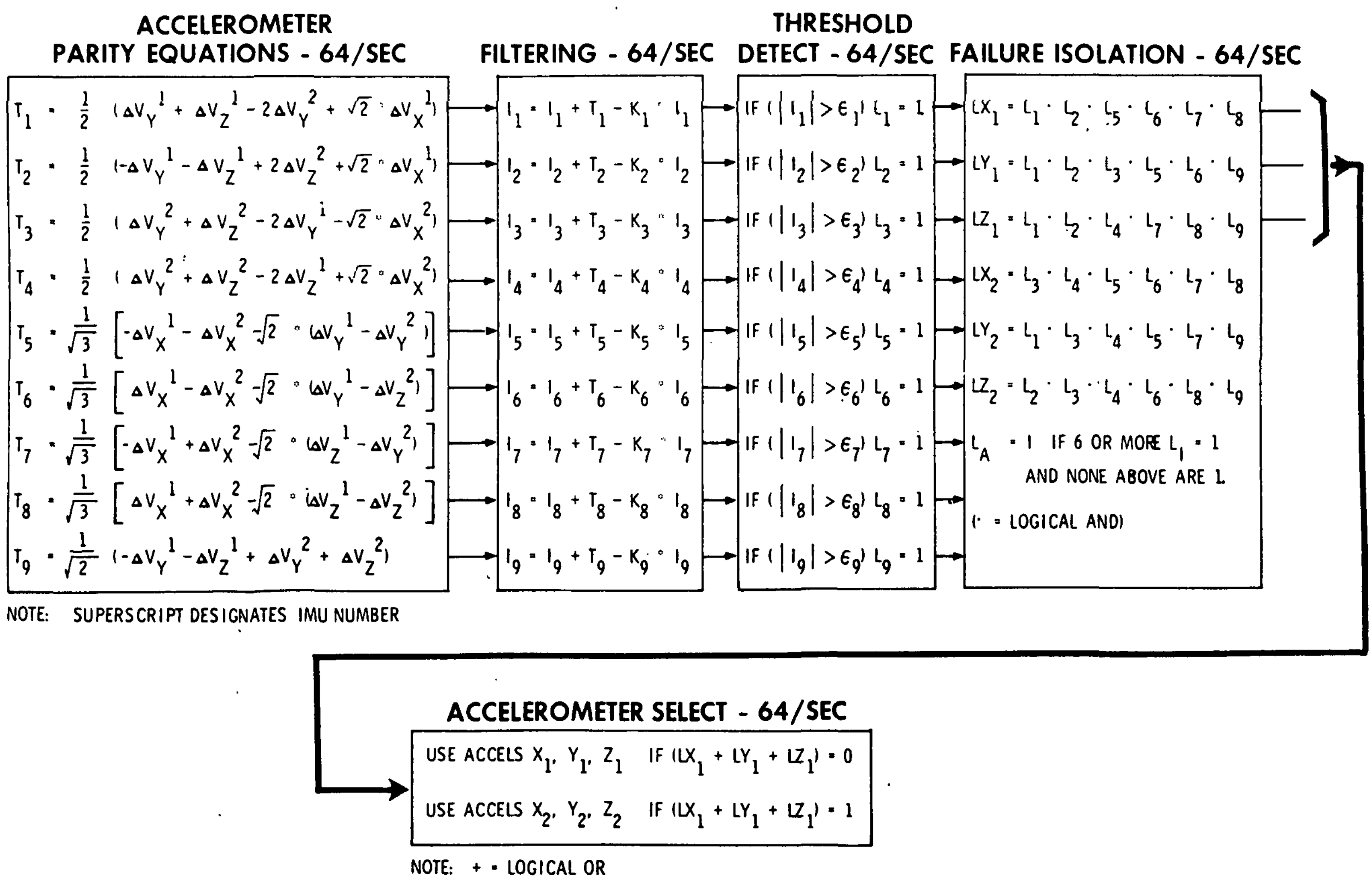

Figure A-5. Accelerometer Failure Detection, Isolation and Selection Equations

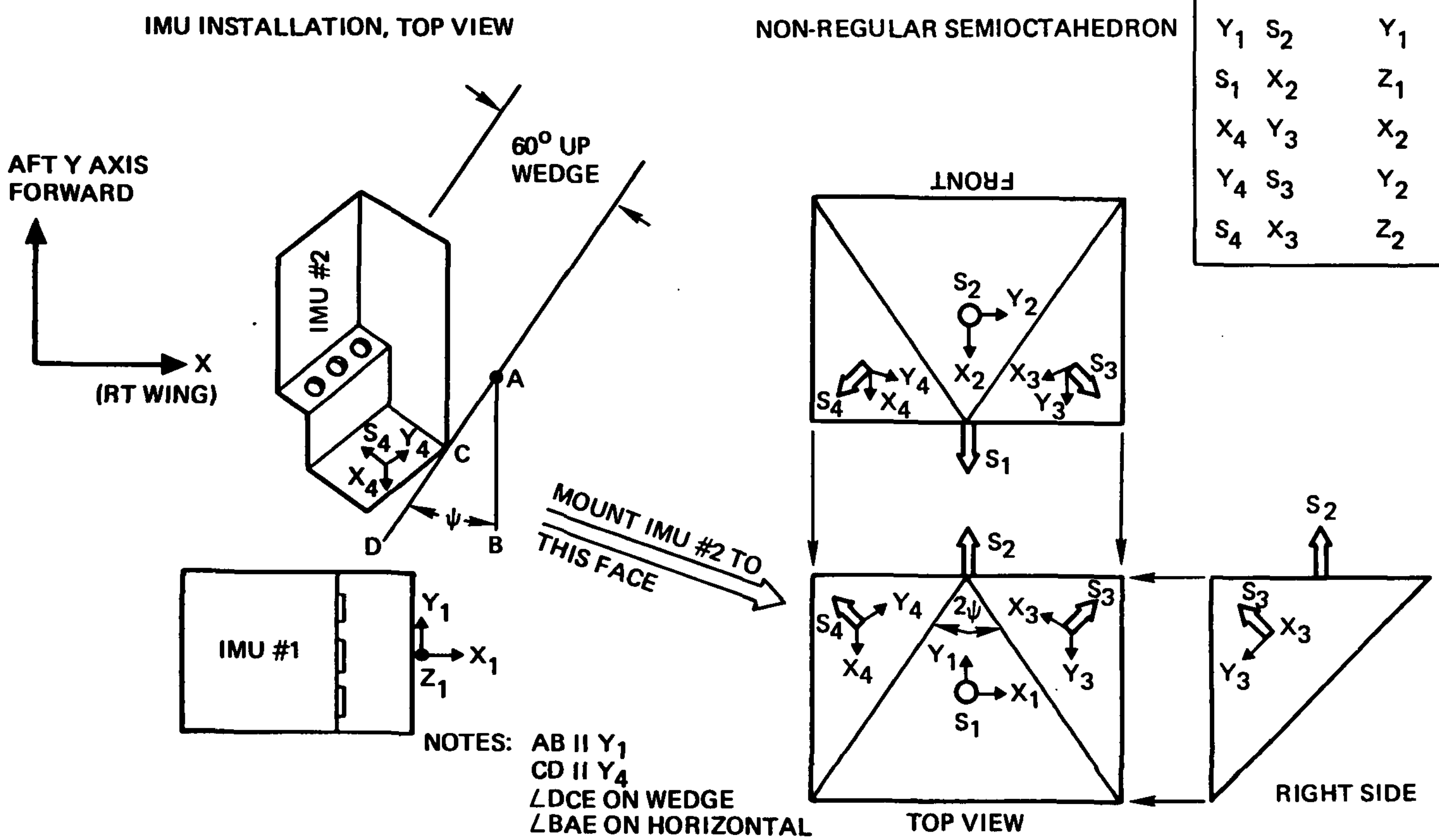

AXIS IDENTITIES		
GYRO	ACCELERO-METER	BODY
X_1 Y_2	X_1	X
Y_1 S_2	Y_1	Y
S_1 X_2	Z_1	Z
X_4 Y_3	X_2	X
Y_4 S_3	Y_2	Y
S_4 X_3	Z_2	Z

NOTES: AB II Y_1
CD II Y_4
∠DCE ON WEDGE
∠BAE ON HORIZONTAL
$\psi = \tan^{-1} \frac{1}{\sqrt{2}} = 35.264^\circ$
S_4 IS IMU #2 "Z" AXIS
S_3 IS IMU #2 "Y" AXIS

Figure A-6. Dual IMU Axis Geometry

DUAL IMU AXIS DEFINITIONS

IMU	SPIN VECTOR	GYRO	SPIN AXIS	X GYRO INPUT AXIS	Y GYRO INPUT AXIS	Z ACCEL.	X ACCEL.	Y ACCEL.
1	S_1	Z_1	(0, 0, 1)	$X_1 = (1, 0, 0)$	$Y_1 = (0, 1, 0)$	$Z_1 = (0, 0, 1)$	$X_1 = (1, 0, 0)$	$Y_1 = (0, 1, 0)$
	S_2	Y_1	(0, 1, 0)	$X_2 = (0, 0, 1)$	$Y_2 = R_1 = (1, 0, 0)$			
2	S_3	Y_2	$\left(\frac{1}{\sqrt{2}}, \frac{1}{2}, \frac{1}{2}\right)$	$X_3 = \left(-\frac{1}{\sqrt{2}}, \frac{1}{2}, \frac{1}{2}\right)$	$Y_3 = R_2 = \left(0, -\frac{1}{\sqrt{2}}, \frac{1}{\sqrt{2}}\right)$	$Z_2 = \left(-\frac{1}{\sqrt{2}}, \frac{1}{2}, \frac{1}{2}\right)$	$X_2 = \left(0, -\frac{1}{\sqrt{2}}, \frac{1}{\sqrt{2}}\right)$	$Y_2 = \left(\frac{1}{\sqrt{2}}, \frac{1}{2}, \frac{1}{2}\right)$
	S_4	Z_2	$\left(-\frac{1}{\sqrt{2}}, \frac{1}{2}, \frac{1}{2}\right)$	$X_4 = \left(0, -\frac{1}{\sqrt{2}}, \frac{1}{\sqrt{2}}\right)$	$Y_4 = \left(\frac{1}{\sqrt{2}}, \frac{1}{2}, \frac{1}{2}\right)$			

EDGE VECTORS

$e_{ij} = (S_i \times S_j)/|S_i \times S_j|$

$e_{12} = (-1, 0, 0)$

$e_{13} = \frac{1}{\sqrt{3}}(-1, \sqrt{2}, 0)$

$e_{14} = \frac{1}{\sqrt{3}}(-1, -\sqrt{2}, 0)$

$e_{23} = \frac{1}{\sqrt{3}}(1, 0, -\sqrt{2})$

$e_{24} = \frac{1}{\sqrt{3}}(1, 0, \sqrt{2})$

$e_{34} = \frac{1}{\sqrt{2}}(0, -1, 1)$

PROJECTION MATRICES

$[S_i] = [I - S_i S_i T]$

$$[S_1] = \begin{bmatrix} 1 & 0 & 0 \\ 0 & 1 & 0 \\ 0 & 0 & 0 \end{bmatrix} \qquad [S_3] = \begin{bmatrix} \frac{1}{2} & -\frac{1}{2\sqrt{2}} & -\frac{1}{2\sqrt{2}} \\ -\frac{1}{2\sqrt{2}} & \frac{3}{4} & -\frac{1}{4} \\ -\frac{1}{2\sqrt{2}} & -\frac{1}{4} & \frac{3}{4} \end{bmatrix}$$

$$[S_2] = \begin{bmatrix} 1 & 0 & 0 \\ 0 & 0 & 0 \\ 0 & 0 & 1 \end{bmatrix} \qquad [S_4] = \begin{bmatrix} \frac{1}{2} & \frac{1}{2\sqrt{2}} & \frac{1}{2\sqrt{2}} \\ \frac{1}{2\sqrt{2}} & \frac{3}{4} & -\frac{1}{4} \\ \frac{1}{2\sqrt{2}} & -\frac{1}{4} & \frac{3}{4} \end{bmatrix}$$

Figure A-7. Dual IMU Axis Definitions

APPENDIX B

RLN-50 NORTH-SOUTH FLIGHT

TEST DATA

14 NOVEMBER 1977

RLN-50 NORTH-SOUTH FLIGHT
14 NOVEMBER 1977

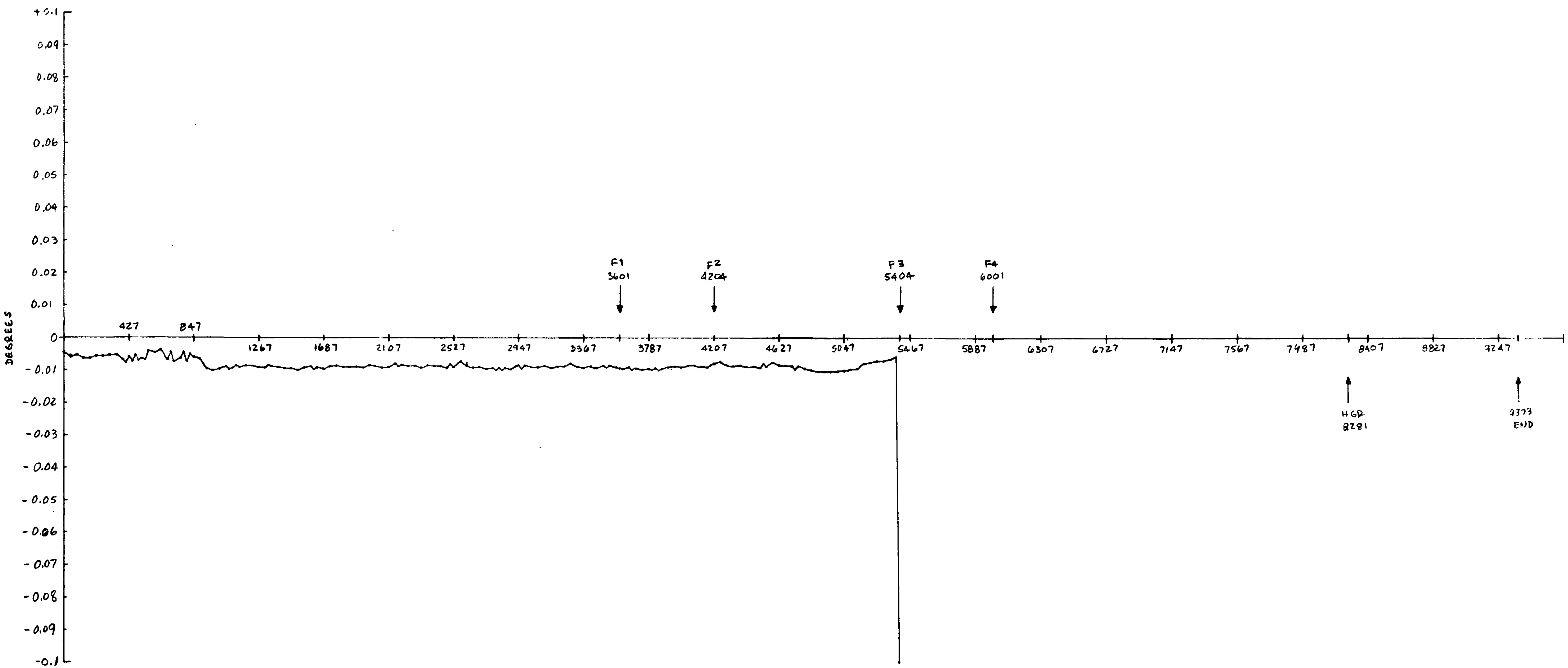

Figure B-1. Gyro Parity Equation T_{12}

RLN-50 NORTH-SOUTH FLIGHT
14 NOVEMBER 1977

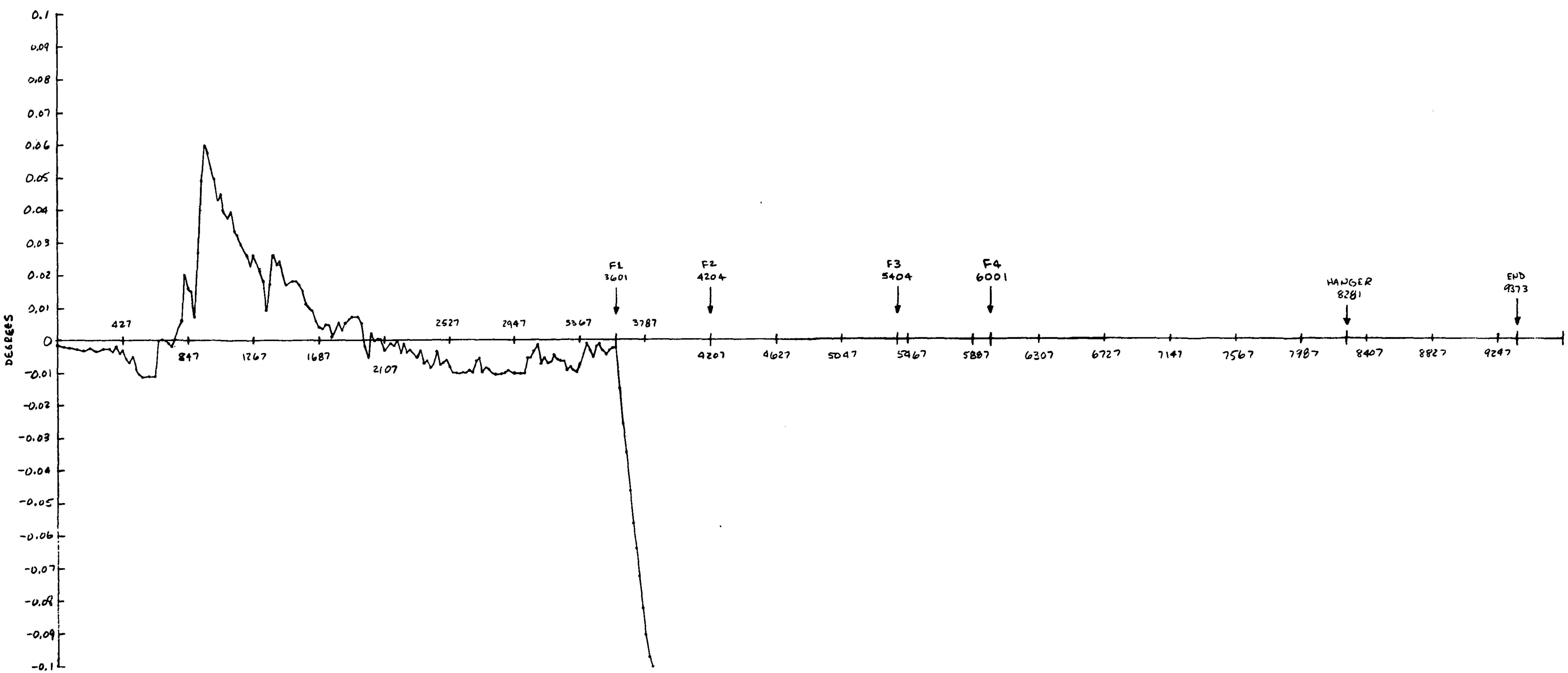

Figure B-2. Gyro Parity Equation T_{13}

RLN-50 NORTH-SOUTH FLIGHT

14 NOVEMBER 1977

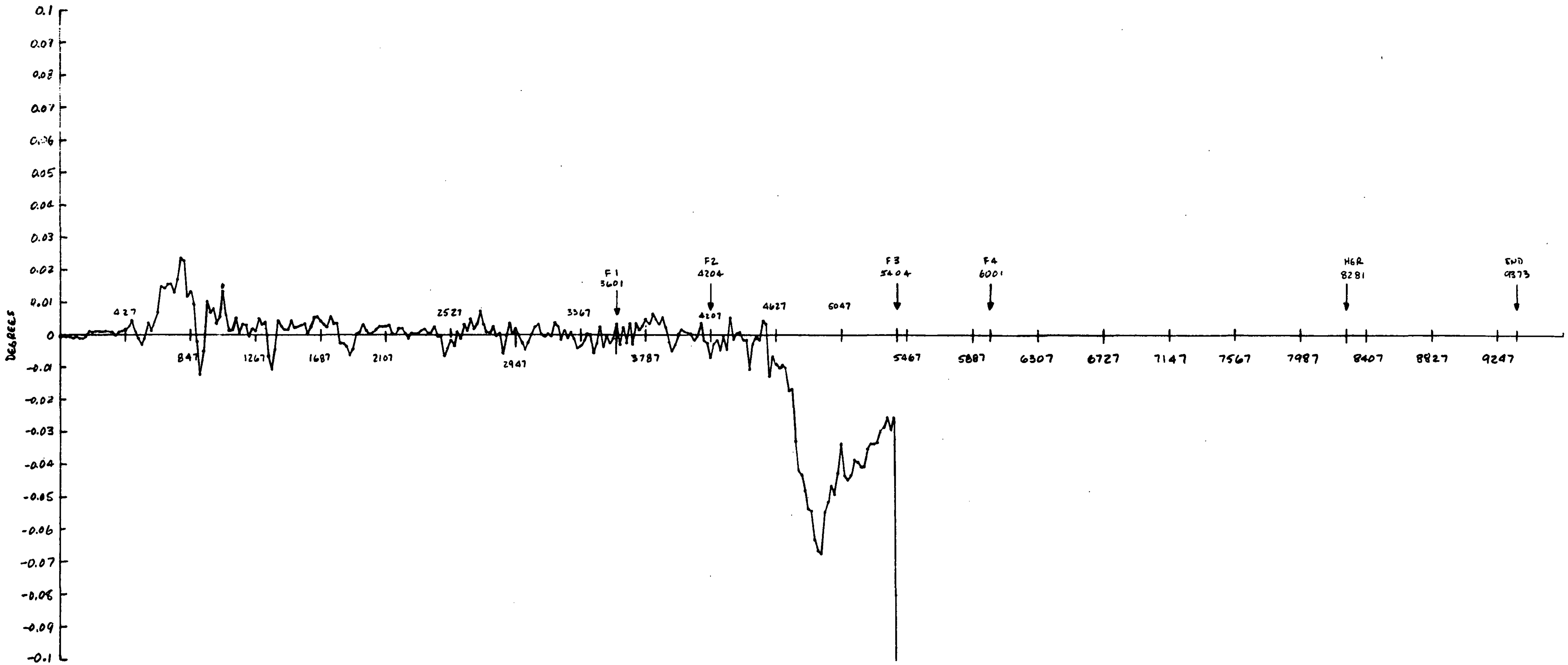

Figure B-3. Gyro Parity Equation T_{14}

RLN-50 NORTH-SOUTH FLIGHT
14 NOVEMBER 1977

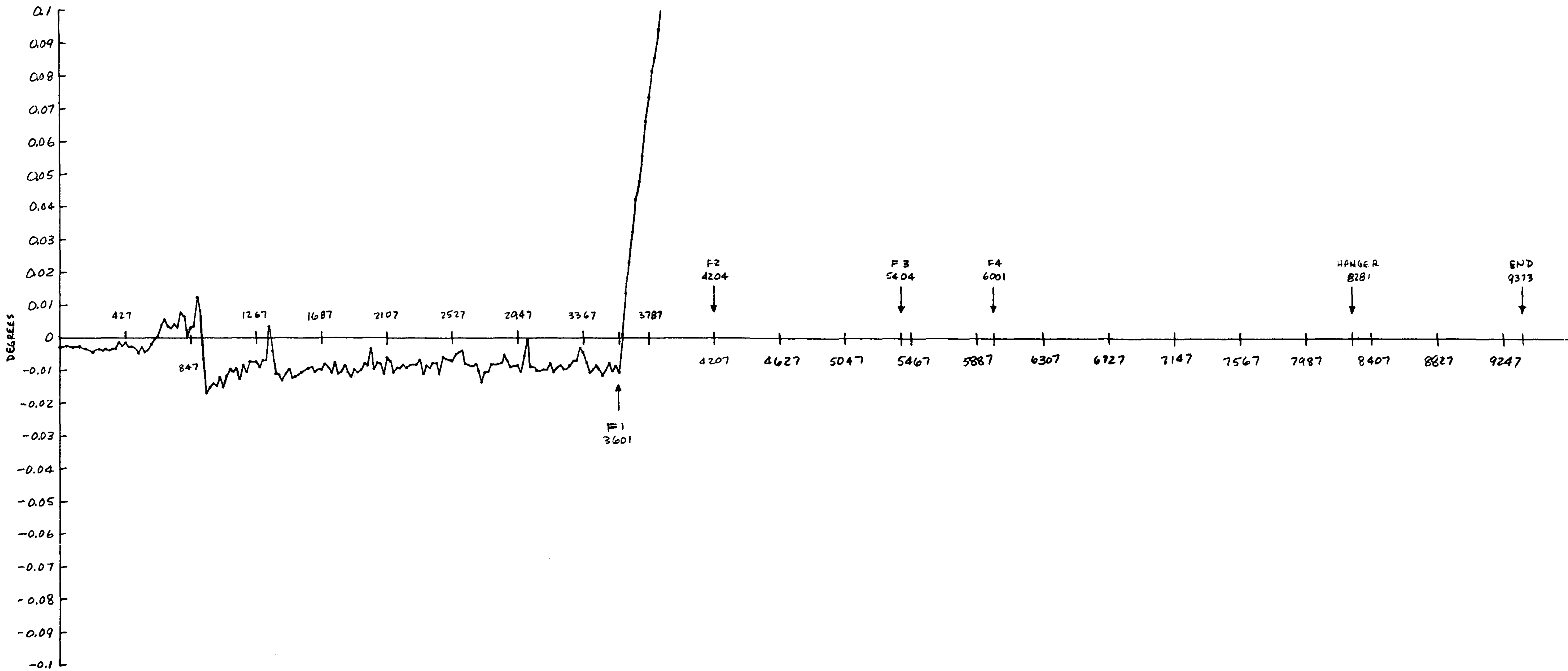

Figure B-4. Gyro Parity Equation T_{23}

RLN-50 NORTH-SOUTH FLIGHT
14 NOVEMBER 1977

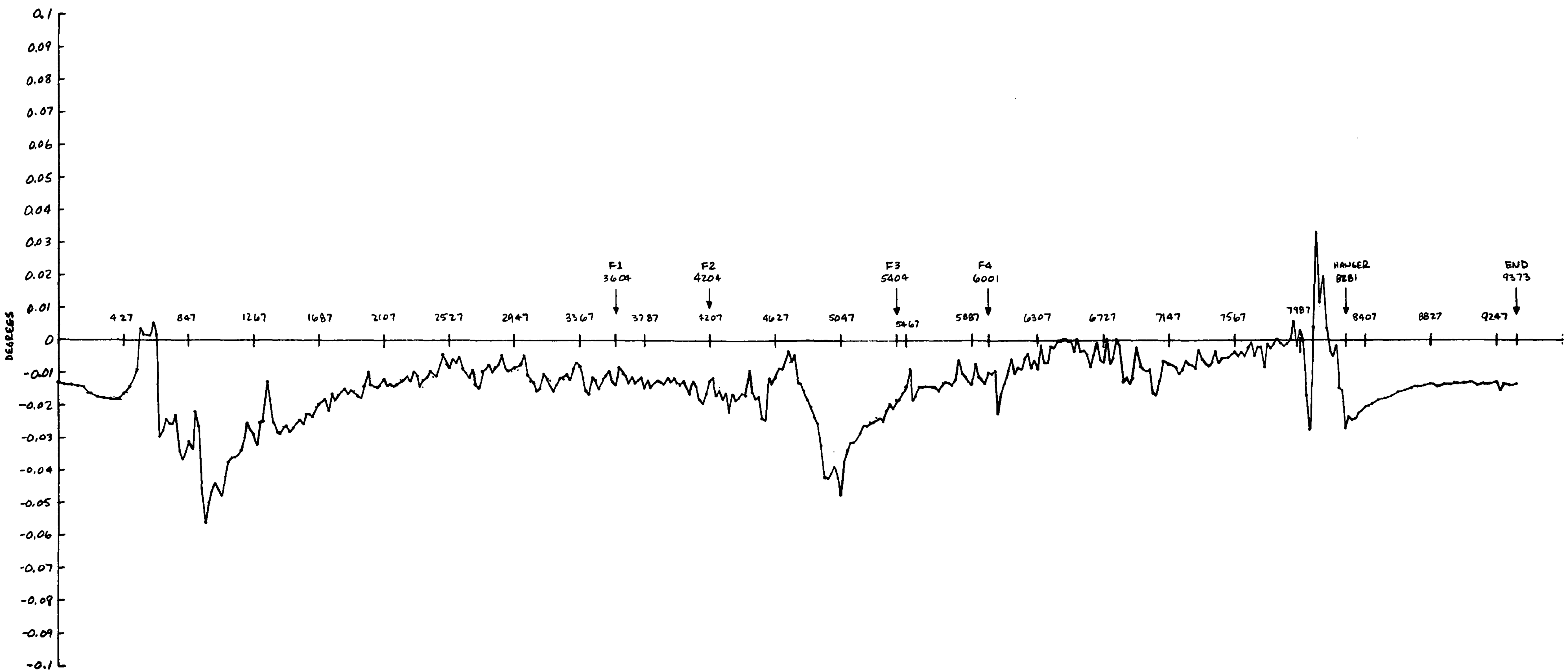

Figure B-5. Gyro Parity Equation T_{24}

RLN-50 NORTH-SOUTH FLIGHT
14 NOVEMBER 1977

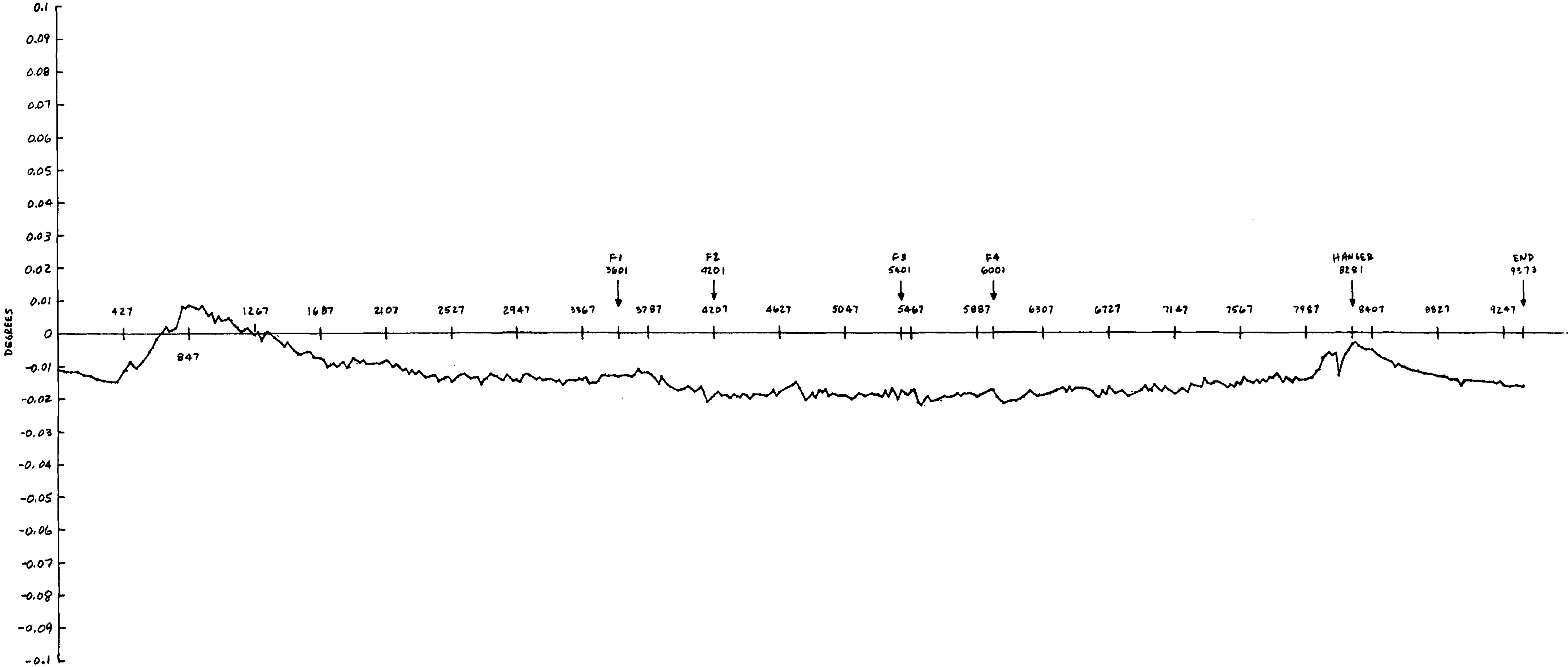

Figure B-6. Gyro Parity Equation T_{34}

RLN-50 NORTH-SOUTH FLIGHT

14 NOVEMBER 1977

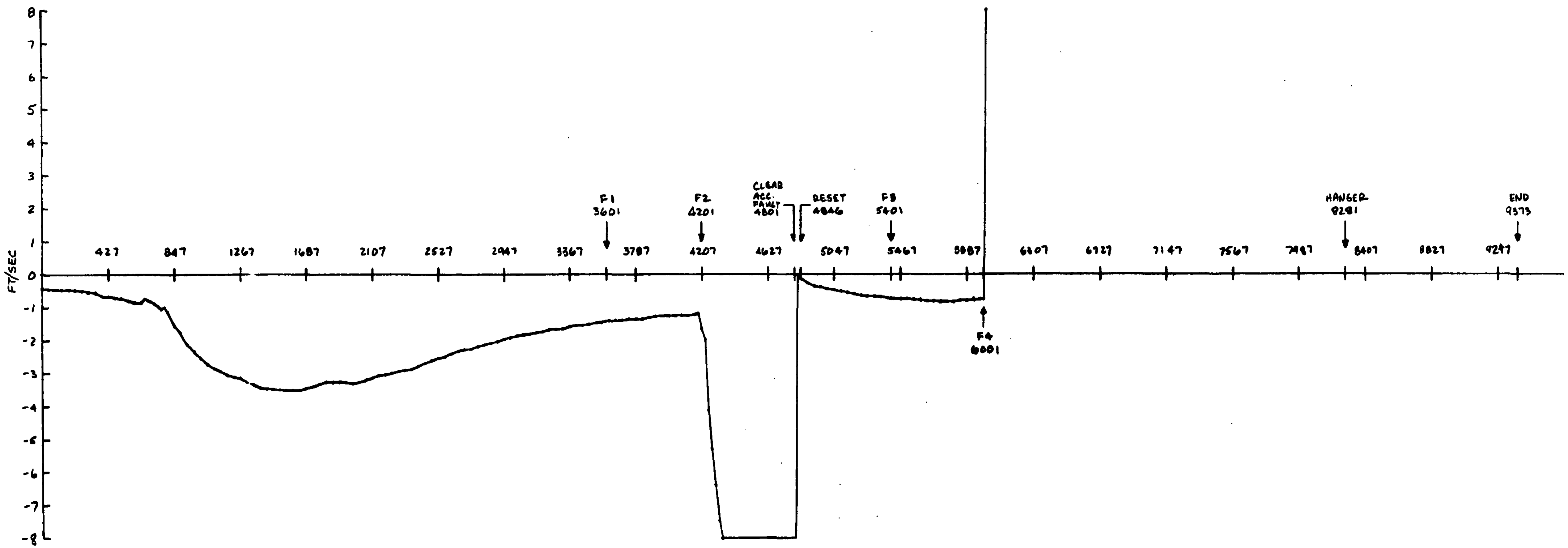

Figure B-7. Accelerometer Parity Equation T_1

RLN-50 NORTH-SOUTH FLIGHT
14 NOVEMBER 1977

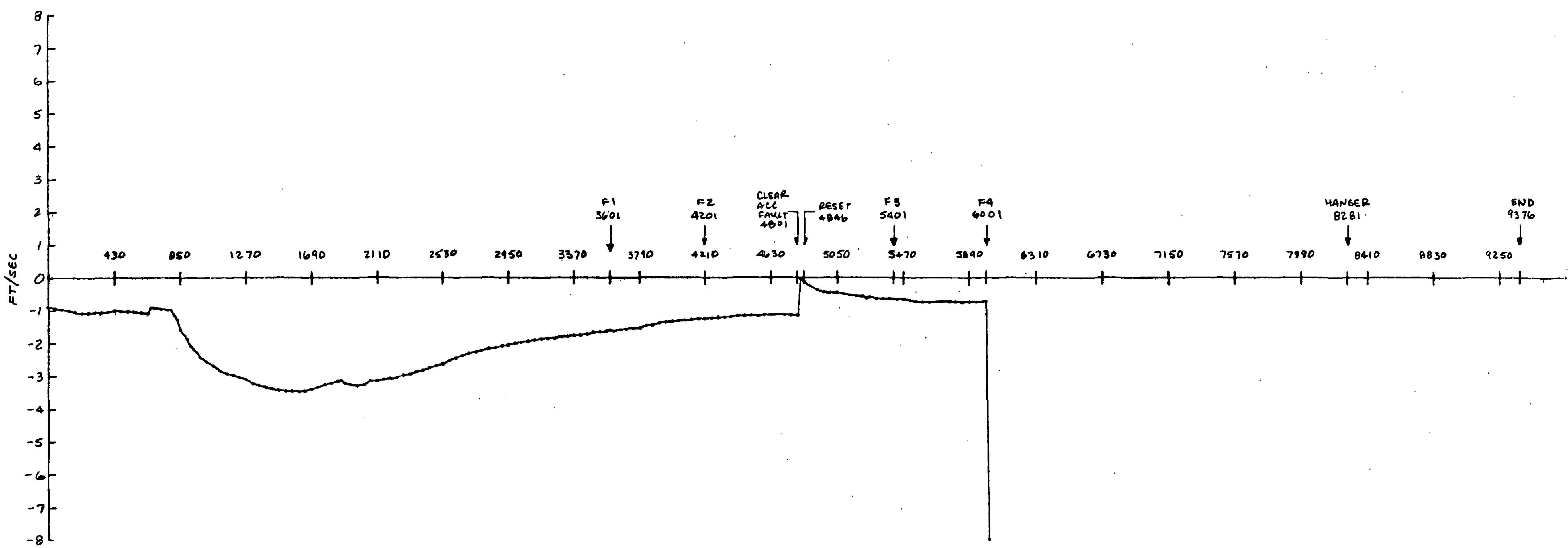

Figure B-8. Accelerometer Parity Equation T_2

RLN-50 NORTH-SOUTH FLIGHT
14 NOVEMBER 1977

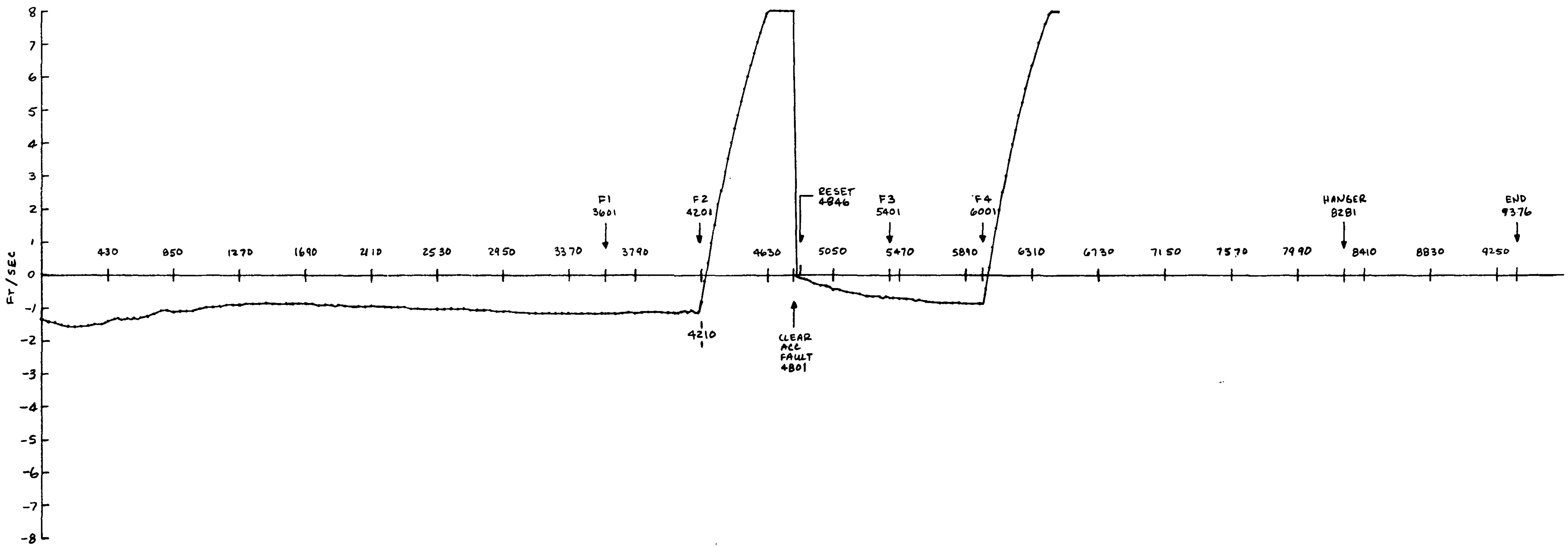

Figure B-9. Accelerometer Parity Equation T_3

RLN-50 NORTH-SOUTH FLIGHT

14 NOVEMBER 1977

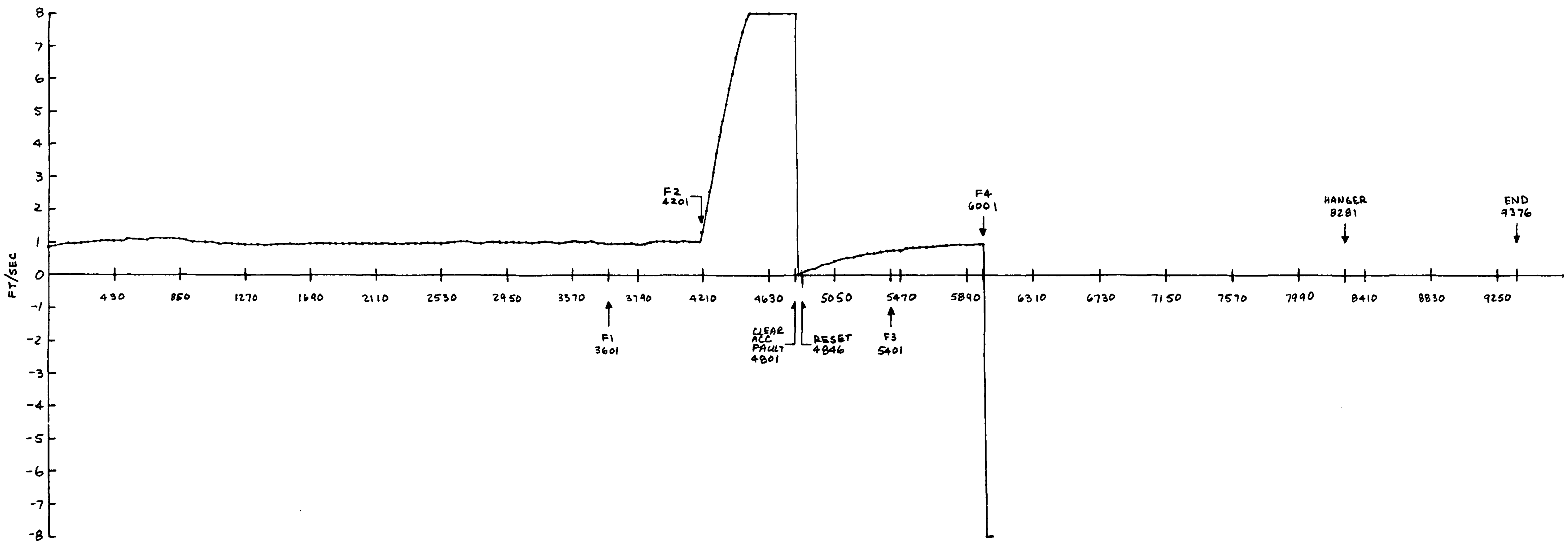

Figure B-10. Accelerometer Parity Equation T_4

RLN-50 NORTH-SOUTH FLIGHT
14 NOVEMBER 1977

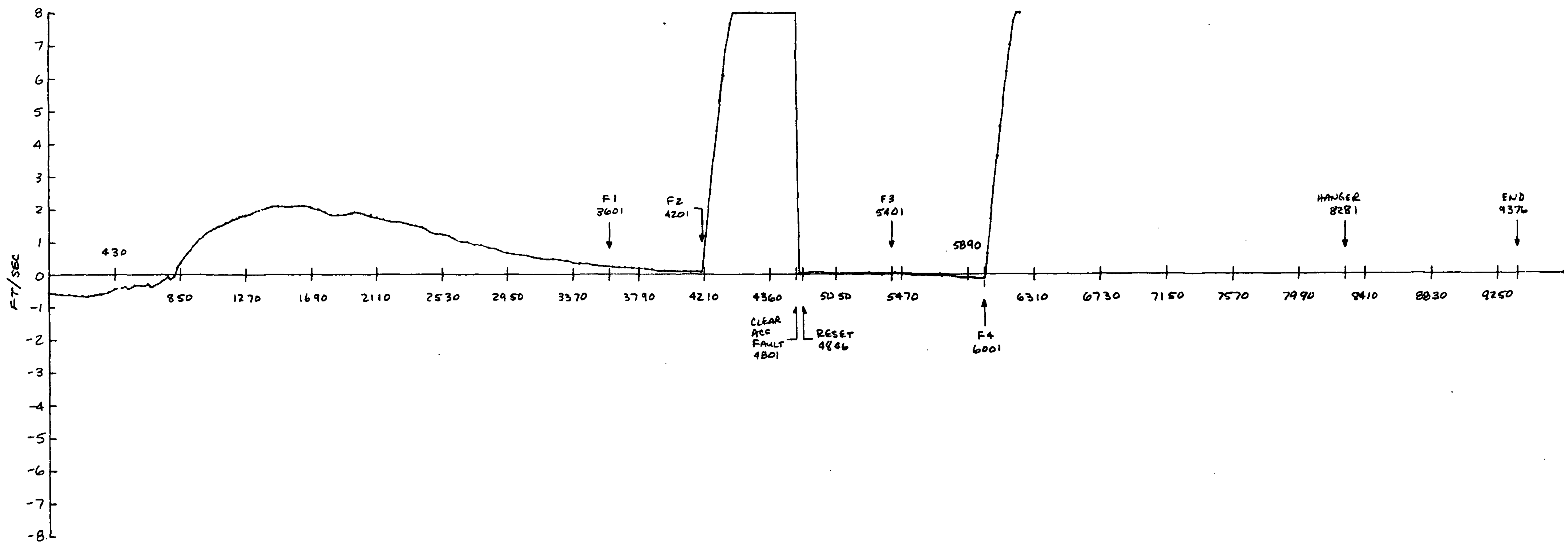

Figure B-11. Accelerometer Parity Equation T_5

RLN-50 NORTH-SOUTH FLIGHT
14 NOVEMBER 1977

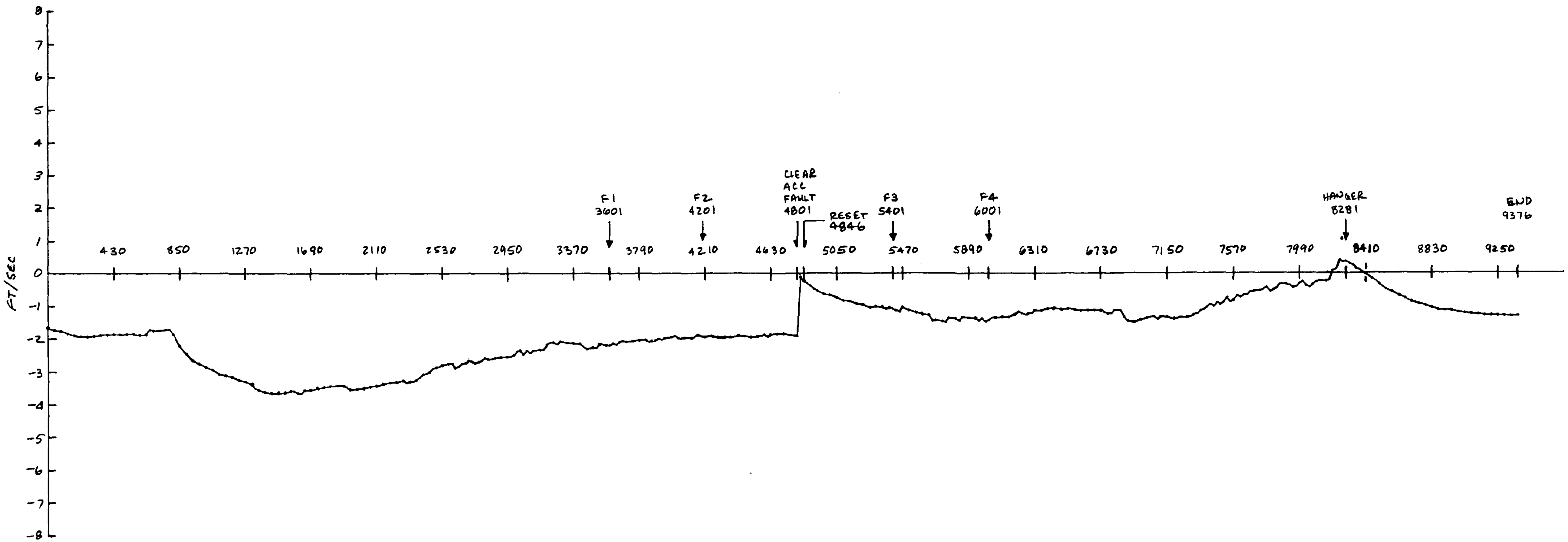

Figure B-12. Accelerometer Parity Equation T_6

RLN-50 NORTH-SOUTH FLIGHT

14 NOVEMBER 1977

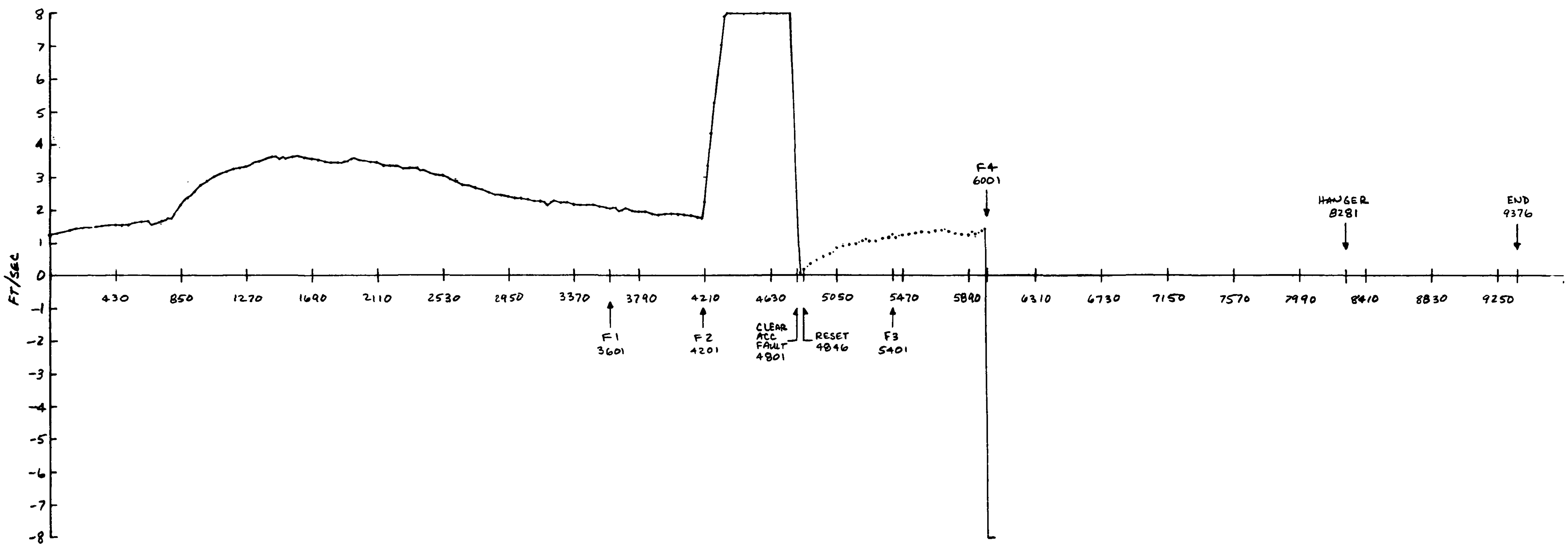

Figure B-13. Accelerometer Parity Equation T_7

RLN-50 NORTH-SOUTH FLIGHT

14 NOVEMBER 1977

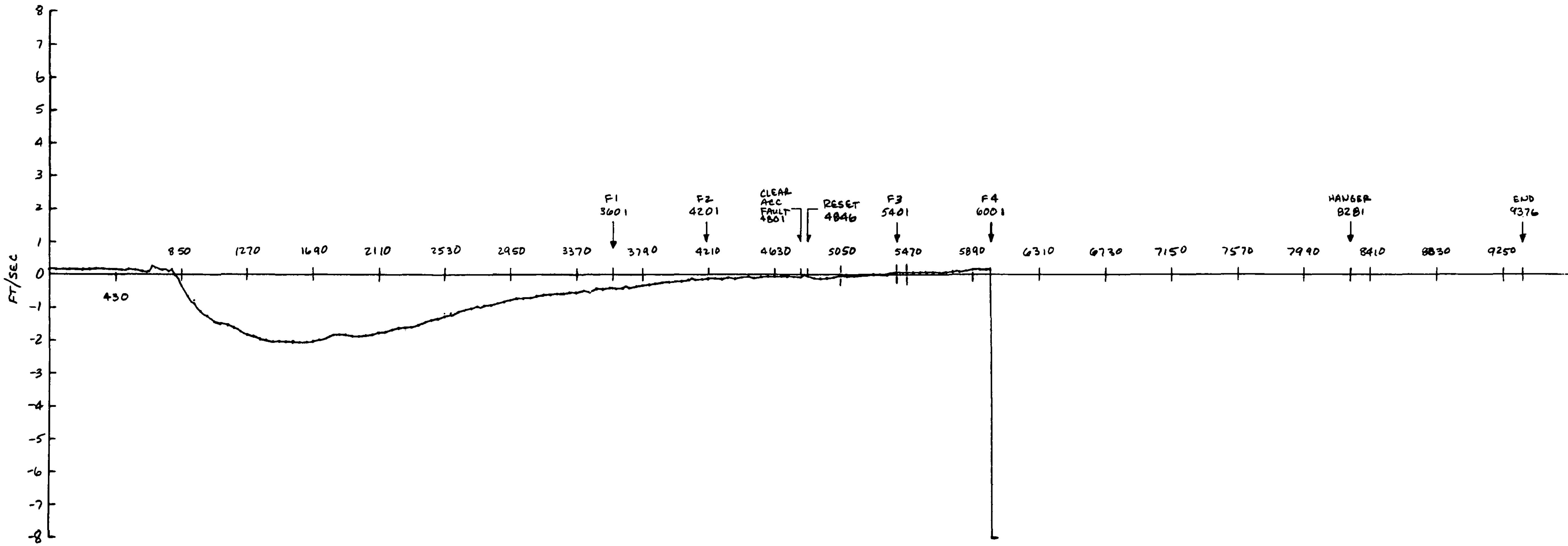

Figure B-14. Accelerometer Parity Equation T_8

RLN-50 NORTH-SOUTH FLIGHT
14 NOVEMBER 1977

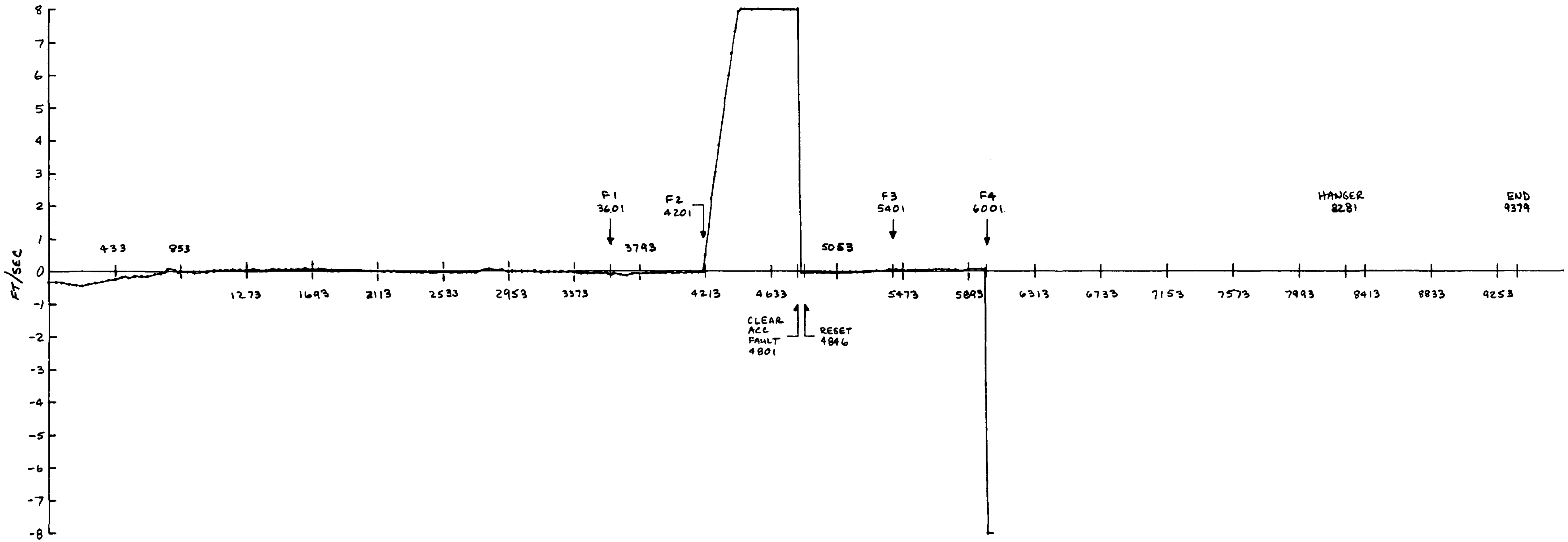

Figure B-15. Accelerometer Parity Equation T_9

TABLE I. TEST PLAN FOR NASA/LANGLEY FLIGHT DEMONSTRATION

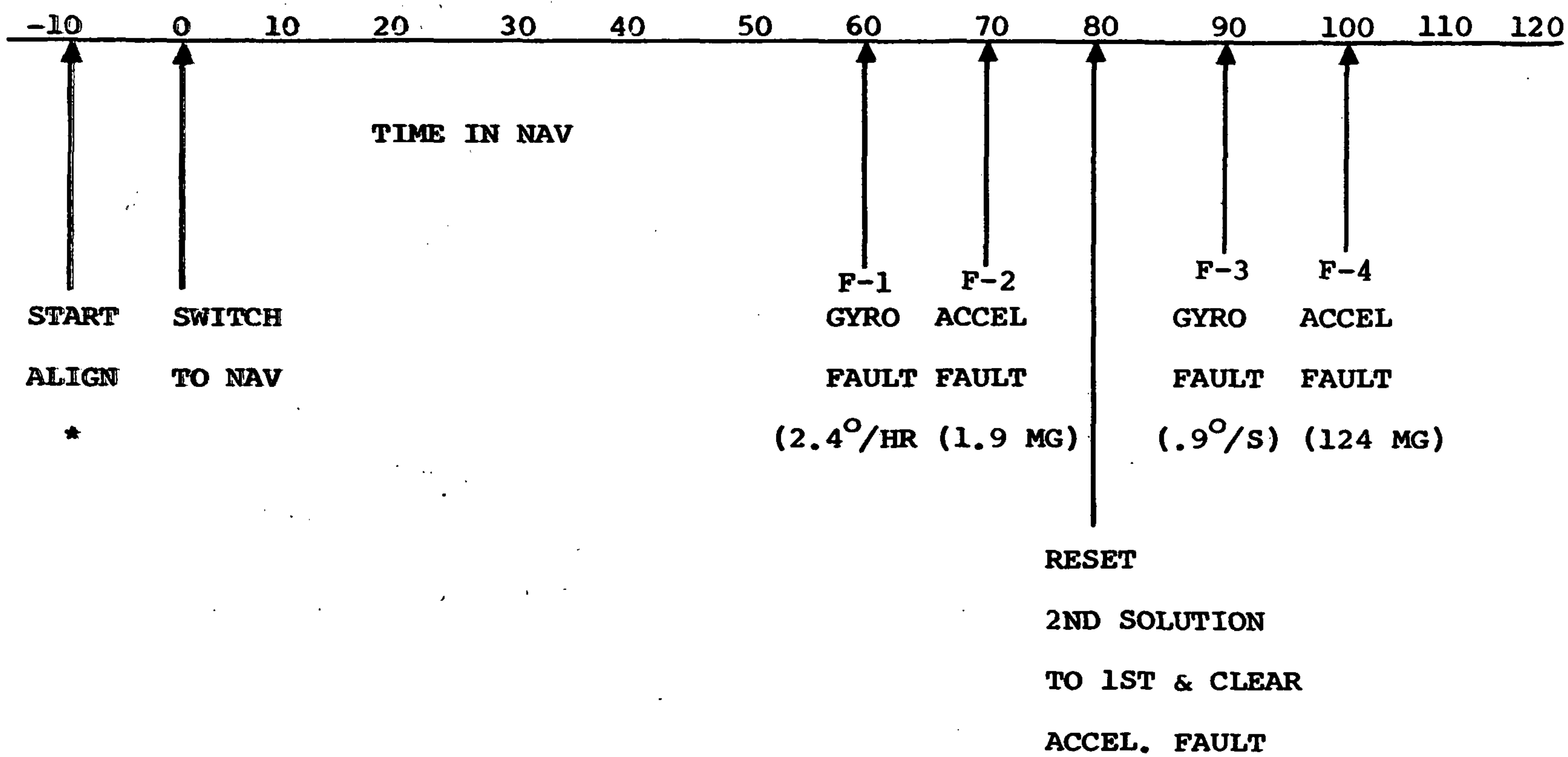

*NOTE: Alternate solution and auto select flags were set at the beginning of the ALIGN mode.